entropy

MDPI

Article

Replica Field Theory for a Generalized Franz–Parisi Potential of Inhomogeneous Glassy Systems: New Closure and the Associated Self-Consistent Equation

Hiroshi Frusawa

Laboratory of Statistical Physics, Kochi University of Technology, Tosa-Yamada, Kochi 782-8502, Japan; frusawa.hiroshi@kochi-tech.ac.jp

Abstract: On approaching the dynamical transition temperature, supercooled liquids show heterogeneity over space and time. Static replica theory investigates the dynamical crossover in terms of the free energy landscape (FEL). Two kinds of static approaches have provided a self-consistent equation for determining this crossover, similar to the mode coupling theory for glassy dynamics. One uses the Morita–Hiroike formalism of the liquid state theory, whereas the other relies on the density functional theory (DFT). Each of the two approaches has advantages in terms of perturbative field theory. Here, we develop a replica field theory that has the benefits from both formulations. We introduce the generalized Franz–Parisi potential to formulate a correlation functional. Considering fluctuations around an inhomogeneous density determined by the Ramakrishnan–Yussouf DFT, we find a new closure as the stability condition of the correlation functional. The closure leads to the self-consistent equation involving the triplet direct correlation function. The present field theory further helps us study the FEL beyond the mean-field approximation.

Keywords: supercooled liquids; replica theory; Franz–Parisi potential; density functional theory; self-consistent equation

check for updates

Citation: Frusawa, H. Replica Field Theory for a Generalized Franz–Parisi Potential of Inhomogeneous Glassy Systems: New Closure and the Associated Self-Consistent Equation. *Entropy* **2024**, *26*, 241. https://doi.org/10.3390/e26030241

Academic Editor: Jürn W.P. Schmelzer

Received: 18 January 2024
Revised: 26 February 2024
Accepted: 5 March 2024
Published: 8 March 2024

Copyright: © 2024 by the author. Licensee MDPI, Basel, Switzerland. This article is an open access article distributed under the terms and conditions of the Creative Commons Attribution (CC BY) license (https://creativecommons.org/licenses/by/4.0/).

1. Introduction

Glass, an amorphous solid with elasticity, has a microscopic structure in which localized particles oscillate around their mean positions of a random lattice [1–6]. The spatial randomness is self-generated by the particle localization that breaks translational symmetry. A remarkable feature of the random structure is that glass microscopically lacks the long-range order and is similar to liquid in terms of density–density correlations [1–6]. As a precursor to the random structure of glass, supercooled liquids show heterogeneity over space and time [1–11]. The dynamical heterogeneity and facilitation [4,7–14] emerges on approaching the dynamical transition temperature (T_d), accompanied by the crossover from relaxational to activated dynamics. For $T > T_d$, transport is not collective on a large scale. For $T \to T_d$, the system gets stuck in a glassy metastable state, and the dynamical behaviors of supercooled liquids exhibit features such as a two-step decay with a first relaxation (β-relaxation) to a plateau followed by a stretched exponential relaxation (α-relaxation) of density fluctuations. Along with this dynamical crossover, the dynamics become progressively heterogeneous and correlated in space. For $T < T_d$, the relaxation times of the two-step decay increase rapidly despite slight changes in the disordered microstructure.

Various theories have tried to explain the dynamical heterogeneity and facilitation, as well as the dynamical crossover at T_d. These include either elasticity theory or kinetically constrained models focusing on the dynamical facilitation [4,12–14], and the mode coupling theory (MCT) [15,16], a dynamical theory relevant when approaching T_d from the liquid phase. The MCT describes the onset of the two-step relaxation above T_d and predicts the divergence of β-relaxation time at T_d. Extension to the inhomogeneous MCT further allows

us to describe a growing dynamical heterogeneity using a time-dependent three-or four-point correlation function [2,7–11]. Yet the dynamical transition temperature T_d is higher than the glass transition temperature observed in simulation and experimental studies. An interpretation of this discrepancy is that a mean-field description of the MCT is beyond the scope of the barrier-dominated dynamics between metastable states, though applicable to the relaxation dynamics within a metastable state. The divergent behavior of the two-step decay predicted by the MCT at T_d becomes incomplete because of the activated events remaining in actual liquids for $T \leq T_d$ [15,16].

The activation dynamics dominant below T_d are due to transitions between metastable states [15–20]. Therefore, the dynamical crossover implies the emergence of many metastable states at T_d or the appearance of a free energy landscape (FEL) characterized by an exponentially large number of metastable states below T_d. From the thermodynamic point of view, we can describe the characteristic of the FEL using the configurational entropy obtained from the logarithm of the number of metastable states [1,2,17–20]. The Adam–Gibbs relation provides results in quantitative agreement with simulation and experimental results, relating the drastic changes in the relaxation time and viscosity to the decrease of the configurational entropy on approaching the glass transition temperature [17–22]. For example, simulation studies on mixtures interacting via the Lennard-Jones potential and its repulsive counterpart, the WCA one, demonstrate that these systems exhibit quite different dynamics despite having nearly identical structures [23–28]. Such a large difference in the dynamics is ascribable to a considerable gap between the configurational entropies while making a slight difference between the two-point correlation functions. Previous investigations confirmed that the configurational entropies associated with correlation functions differ greatly between the Lennard-Jones and WCA mixtures despite the structural similarity, therefore predicting the distinct dynamical behaviors from the Adam–Gibbs relation [23–28].

Static approaches, other than dynamical ones such as the MCT, are relevant to investigate the FEL or the configurational entropy [17–20,29–57]. These include replica theory [17–20,29–38], density functional theory (DFT) [39–52], and a combination of the replica theory and DFT [53–57]. The static theories commonly focus on local minima of free-energy functionals without considering fluctuations due to the mean-field approximation. On the one hand, the DFT determines the metastable state by exploring a local minimum of the free-energy density functional [39–52]. Given the inhomogeneous density distribution as overlapping Gaussians centered around a random lattice, previous studies have confirmed that Gaussian distribution with a large spread creates the optimum density profile. The low degree of localization around the random lattice is consistent with experimental and simulation results. On the other hand, replica theory considers a system of coupled m-replicas of the original system [17–20,29–38,53–57]. The replica free-energy functional depends on a two-point correlation function between two copies (an inter-replica correlation function), an order parameter measuring the degree of similarity between two typical configurations. We obtain the correct result by taking the limit of $m \to 1$ with the inter-replica coupling switched off. While the order parameter goes to zero in the liquid state without the inter-replica coupling, the order parameter in an ergodicity-broken phase has a finite value because two copies remain highly correlated even after switching off the inter-replica coupling. The replica theory has successfully explained experimental and simulation results using the following four approximations: the small cage expansion [17–20,31,32], the effective potential approximation [17–20,31,32], the replicated hypernetted-chain (RHNC) approximation [33–38], and the third-order functional expansion in DFT [56–61]. While the first two are perturbation methods with the local cage size as a reference scale, the last two approximations cover those of the liquid-state theory [62–64].

The Franz–Parisi (FP) potential obtained in the RHNC approximation serves as a starting point for this paper. The FP potential [65–75] is a function of overlap Q, a weighted average over the system of the two-point correlation function, and plays the same role as the Landau free energy of a global parameter Q that indicates a distance between the

two copies in configuration space. Theoretical and simulation studies have demonstrated that the FP potential reproduces the temperature evolution of FELs, just like the Landau free energy [65–75]. With decreasing temperature, the FP potential develops a secondary minimum for $Q > 0$ representing a metastable state. Considering $Q = 0$ in the liquid state, we can see that the potential difference, $V(Q) - V(0)$, corresponds to the entropic cost of localizing the system in a single metastable state (i.e., the configurational entropy).

In this paper, we generalize the FP potential by fixing an inter-replica correlation function instead of the overlap Q. We formulate the generalized FP potential by developing a new framework that is beneficial to investigate the FEL while considering inhomogeneous supercooled liquids with the help of field theoretical method. A field theory combining the DFT [53–61] and replica theory [17–20,29–38,53–57] forms the basis of our framework. There are two requirements to be satisfied by the field theory and the associated functional. The first requirement is that the developed framework can consider inhomogeneous systems. The second requirement is that the generalized FP functional applies to non-equilibrium states away from metastable states. To meet the requirements, this paper presents the correlation functional theory that provides the generalized FP potential functional without going through the Morita-Hiroike functional [33–38,62–64]. The generalized FP potential has three features as a functional of density and correlation function. First, this potential is a functional of metastable density that becomes equal to that of the DFT in the limit of $m \to 1$. Second, the field-theoretical perturbation method allows us to have a new correlation functional different from the Morita–Hiroike one while maintaining consistency with the liquid theory in that the approximate form reduces to the RHNC functional. Last, the potential functional of a given inter-replica correlation function has a minimum where a new closure reducible to the RHNC approximation [33–38,62,63] holds. A remarkable result is that an approximation of the new closure yields the self-consistent equation for a non-ergodicity parameter that includes the triplet direct correlation function (DCF) [62,63,76–78], similar to that formulated by either the MCT [15,16] or the replica theory [37,56,57], respectively.

The paper is organized as follows. In Section 2, we define the generalized FP potential. Comparison between the generalized and original FP potentials clarifies what we modify through the generalization. Section 3 summarizes the theoretical results consisting of four parts as follows: relation for obtaining the generalized FP potential from the grand potential of m-replica system with inter-replica correlation function fixed (*Result 1*); functional form of the constrained grand potential (*Result 2*); new closure for two-point correlation function (*Result 3*); the associated self-consistent equation for a non-ergodicity parameter (*Result 4*). We obtain the generalized FP potential from *Result 2* with the help of the relation in *Result 1*. The extremum condition of this potential yields a new closure in *Result 3*. It also turns out that a self-consistent equation obtained from an approximate form of the closure involves the triplet DCF as presented in *Result 4*. In Section 4, we calculate the perturbative terms using a strong-coupling perturbation theory developed for obtaining *Result 2* (see Appendix B). In the saddle-point approximation, the strong-coupling perturbation theory provides the correlation functional form of the constrained grand potential given in *Result 2*. In Section 5, we make some concluding remarks.

2. Generalized Franz–Parisi (FP) Potential

We generalize the FP potential in comparison with its original definition.

2.1. The Original FP Potential

Let $\mathcal{C}_a$ be a configuration that represents a set of N-particle positions, $\{\boldsymbol{r}_{a,i}\}_{i=1,\cdots,N}$, in replica a ($1 \le a \le m$) when considering m copies of the liquid. The overlap $\widehat{Q}(\widehat{\rho}_a, \widehat{\rho}_b)$ ($a \ne b$) measures the degree of similarity between a pair of replicas using the microscopic

density (or the so-called density "operator" [79–88]) in replica a, $\widehat{\rho}_a^{(N)}(\boldsymbol{r}) = \sum_{i=1}^{N} \delta(\boldsymbol{r} - \boldsymbol{r}_{a,i})$. We define that

$$\widehat{Q}(\widehat{\rho}_a, \widehat{\rho}_b) = \frac{1}{N} \iint d\boldsymbol{r}\, d\boldsymbol{r}' \widehat{\rho}_a^{(N)}(\boldsymbol{r}) \widehat{\rho}_b^{(N)}(\boldsymbol{r}') \eta(\boldsymbol{r} - \boldsymbol{r}'), \tag{1}$$

where a distribution function $\eta(\boldsymbol{r})$ specifies the spatial averaging performed over a finite range; for example, we have $\eta(\boldsymbol{r}) = \Theta(a - |\boldsymbol{r}|)$ using the Heaviside function $\Theta(r)$ and particle diameter a [65–75].

The FP potential $V(Q)$ is obtained in two steps [65–75]. First, we fix a reference configuration $\widehat{\rho}_1$ of replica 1, which plays the role of quenched variable in the effective potential $V(Q, \widehat{\rho}_1)$ as seen from the following definition:

$$e^{-\beta N V^+(Q, \widehat{\rho}_1)} = \sum_{\mathcal{C}_a} e^{-\beta U_a(\widehat{\rho}_1, \widehat{\rho}_a)} \delta\Big[Q - \widehat{Q}(\widehat{\rho}_1, \widehat{\rho}_a) \Big], \tag{2}$$

$$V(Q, \widehat{\rho}_1) = \lim_{U_{\text{inter}} \to 0} V^+(Q, \widehat{\rho}_1), \tag{3}$$

where $\sum_{\mathcal{C}_a}$ denotes $(1/N!) \int \cdots \int d\boldsymbol{r}_{a,1} \cdots d\boldsymbol{r}_{a,N}$ in the canonical ensemble of replica a for $a \geq 2$, β the inverse thermal energy $(k_B T)^{-1}$, and $U_a(\widehat{\rho}_1, \widehat{\rho}_a)$ the interaction energy of replica a that is the sum of intra-replica interaction energy $U_{\text{intra}}(\widehat{\rho}_a)$ and inter-replica one $U_{\text{inter}}(\widehat{\rho}_1, \widehat{\rho}_a)$:

$$U_a(\widehat{\rho}_1, \widehat{\rho}_a) = U_{\text{intra}}(\widehat{\rho}_a) + U_{\text{inter}}(\widehat{\rho}_1, \widehat{\rho}_a), \tag{4}$$

where

$$U_{\text{intra}}(\widehat{\rho}_a) = \frac{1}{2} \iint d\boldsymbol{r} d\boldsymbol{r}' \Big\{ \widehat{\rho}_a^{(N)}(\boldsymbol{r}) v(\boldsymbol{r} - \boldsymbol{r}') \widehat{\rho}_a^{(N)}(\boldsymbol{r}') - \widehat{\rho}_a^{(N)}(\boldsymbol{r}) v(\boldsymbol{r} - \boldsymbol{r}') \delta(\boldsymbol{r} - \boldsymbol{r}') \Big\}, \tag{5}$$

$$U_{\text{inter}}(\widehat{\rho}_1, \widehat{\rho}_a) = \iint d\boldsymbol{r} d\boldsymbol{r}' \widehat{\rho}_1^{(N)}(\boldsymbol{r}) \widetilde{v}(\boldsymbol{r} - \boldsymbol{r}') \widehat{\rho}_a^{(N)}(\boldsymbol{r}'), \tag{6}$$

using the intra-replica interaction potential $v(\boldsymbol{r})$ and the inter-replica one $\widetilde{v}(\boldsymbol{r})$. It is noted that the effective potential $V(Q, \widehat{\rho}_1)$ is defined in the absence of inter-replica interactions as represented by Equation (3).

Next, we perform the canonical average of $V(Q, \widehat{\rho}_1)$ over all possible choices for the reference configuration with the statistical weight $p_{\text{eq}}(\widehat{\rho}_1)$ as follows:

$$V(Q) = \sum_{\mathcal{C}_1} p_{\text{eq}}(\widehat{\rho}_1)\, V(Q, \widehat{\rho}_1), \tag{7}$$

$$p_{\text{eq}}(\widehat{\rho}_1) = \frac{e^{-\beta U_{\text{intra}}(\widehat{\rho}_1)}}{\sum_{\mathcal{C}_1} e^{-\beta U_{\text{intra}}(\widehat{\rho}_1)}}. \tag{8}$$

The replica trick allows us to calculate Equation (7), thus obtaining the FP potential $V(Q)$ of the Landau type.

2.2. Generalization

Here, we introduce a generalized FP potential $W(\widetilde{G})$ as a functional of prescribed correlation function $\widetilde{G}(\boldsymbol{r}, \boldsymbol{r}')$, instead of the overlap Q. In terms of the Landau theory, we consider a local order parameter, instead of the global one. We use the grand canonical ensemble represented by the following operator:

$$\mathrm{Tr}_a \equiv \sum_{N=0}^{\infty} \frac{e^{N\beta\mu}}{N!} \int d\boldsymbol{r}_{a,1} \cdots \int d\boldsymbol{r}_{a,N} = \sum_{N=0}^{\infty} e^{N\beta\mu} \sum_{\mathcal{C}_a}, \tag{9}$$

where the chemical potential $\beta\mu$ in units of $k_B T$ determines the most probable number N^*, thereby providing the uniform density $\overline{\rho} = N^*/V$ common to each replica with volume V.

Given a reference configuration $\mathcal{C}_1$ of replica 1, we have the interaction energy $U_a(\widehat{\rho}_1, \widehat{\rho}_a)$ of replica a, providing the grand potential $\omega_a(\widehat{\rho}_1)$ of replica a as follows:

$$\begin{aligned} e^{-\beta\omega_a^+(\widehat{\rho}_1)} &= \mathrm{Tr}_a\, e^{-\beta U_a(\widehat{\rho}_1,\widehat{\rho}_a)} \\ &= \int D\widetilde{G}\, \mathrm{Tr}_a\, e^{-\beta U_a(\widehat{\rho}_1,\widehat{\rho}_a)} \prod_{b=1,a} \mathcal{I}_b(\rho,\widehat{\rho})\, \Delta_a(\widetilde{G},\rho) \\ &= \int D\widetilde{G}\, e^{-\beta N^* W(\widetilde{G},\widehat{\rho}_1)}, \end{aligned} \tag{10}$$

$$\omega_a(\widehat{\rho}_1) = \lim_{U_{\mathrm{inter}}\to 0} \omega_a^+(\widehat{\rho}_1), \tag{11}$$

where the functional integral representation in Equation (10) is obtained from multiplying the right-hand side (rhs) of the first line in Equation (10) by the following identity:

$$\begin{aligned} 1 &= \int D\widetilde{G} \prod_{b=1,a} \int D\rho_b \prod_{\{\boldsymbol{r}\},\{\boldsymbol{r}'\}} \prod_{\{\boldsymbol{r}\}} \delta\Big[\rho_b(\boldsymbol{r}) - \widehat{\rho}_b^{(N)}(\boldsymbol{r})\Big]\, \delta\Big[\widetilde{G}(\boldsymbol{r},\boldsymbol{r}') - \rho_1(\boldsymbol{r})\rho_a(\boldsymbol{r}')\Big] \\ &= \int D\widetilde{G} \prod_{b=1,a} \mathcal{I}_b(\rho,\widehat{\rho})\, \Delta_a(\widetilde{G},\rho). \end{aligned} \tag{12}$$

Equation (12) implies that

$$\mathcal{I}_b(\rho,\widehat{\rho}) \equiv \int D\rho_b \prod_{\{\boldsymbol{r}\}} \delta\Big[\rho_b(\boldsymbol{r}) - \widehat{\rho}_b^{(N)}(\boldsymbol{r})\Big] = 1, \tag{13}$$

$$\Delta_a(\widetilde{G},\rho) \equiv \prod_{\{\boldsymbol{r}\},\{\boldsymbol{r}'\}} \delta\Big[\widetilde{G}(\boldsymbol{r},\boldsymbol{r}') - \rho_1(\boldsymbol{r})\rho_a(\boldsymbol{r}')\Big]. \tag{14}$$

The relation (13) at $b = 1$ represents that only the density distribution $\widehat{\rho}_1^{(N)}(\boldsymbol{r})$ is allowed due to a fixed configuration $\mathcal{C}_1$ of replica 1.

Equations (10)–(14) reveal that the field-theoretical formulation of the effective potential $W(\widetilde{G},\widehat{\rho}_1)$ can be developed as follows [79–88]:

$$W(\widetilde{G},\widehat{\rho}_1) = \lim_{U_{\mathrm{inter}}\to 0} W^+(\widetilde{G},\widehat{\rho}_1), \tag{15}$$

where

$$\begin{aligned} e^{-\beta N^* W^+(\widetilde{G},\widehat{\rho}_1)} &= \mathrm{Tr}_a\, e^{-\beta U_a(\widehat{\rho}_1,\widehat{\rho}_a)} \prod_{b=1,a} \mathcal{I}_b(\rho,\widehat{\rho})\, \Delta_a(\widetilde{G},\rho) \\ &= \mathcal{I}_1(\rho,\widehat{\rho})\, \mathrm{Tr}_a\, \mathcal{I}_a(\rho,\widehat{\rho})\, e^{-\beta U_a(\rho_1,\rho_a)}\, \Delta_a(\widetilde{G},\rho) \\ &= \mathcal{I}_1(\rho,\widehat{\rho}) \int D\rho_a\, e^{-\beta U_a(\rho_1,\rho_a)}\, \mathrm{Tr}_a \prod_{\{\boldsymbol{r}\}} \delta\Big[\rho_a(\boldsymbol{r}) - \widehat{\rho}_a^{(N)}(\boldsymbol{r})\Big]\, \Delta_a(\widetilde{G},\rho) \\ &= \mathcal{I}_1(\rho,\widehat{\rho}) \int D\rho_a\, e^{-\beta\left\{U_a(\rho_1,\rho_a) - T\mathcal{S}_a^{\mathrm{id}}(\rho_a)\right\}}\, \Delta_a(\widetilde{G},\rho). \end{aligned} \tag{16}$$

In the last line of Equation (16), we have the ideal gas entropy defined by

$$-T\mathcal{S}_a^{\mathrm{id}}(\rho_a) = k_B T \int d\boldsymbol{r}\, \rho_a(\boldsymbol{r})\{\ln\rho_a(\boldsymbol{r}) - 1 - \beta\mu\}. \tag{17}$$

The generalized FP potential $W(\widetilde{G})$ is obtained from the grand canonical average of $W(\widetilde{G},\widehat{\rho}_1)$ for the reference configuration as follows:

$$W(\widetilde{G}) = \mathrm{Tr}_1\, P_{\mathrm{eq}}(\widehat{\rho}_1) W(\widetilde{G},\widehat{\rho}_1), \tag{18}$$

$$P_{\mathrm{eq}}(\widehat{\rho}_1) = \frac{e^{-\beta U_{\mathrm{intra}}(\widehat{\rho}_1)}}{\mathrm{Tr}_1\, e^{-\beta U_{\mathrm{intra}}(\widehat{\rho}_1)}}, \tag{19}$$

similar to Equations (7) and (8). Equation (18) clarifies that a given configuration $\widehat{\rho}_1$ plays a role of quenched disorder to another replica a [65–75]. Since we consider all possible configurations of $\widehat{\rho}_1$, the statistical weight $P_{\rm eq}(\widehat{\rho}_1)$ is of the Boltzmann form as well as $p_{\rm eq}(\widehat{\rho}_1)$ in Equation (8).

Several remarks on Equations (13)–(19) are in order:

- Equation (14) tells us that a prescribed correlation field $\widetilde{G}(\boldsymbol{r},\boldsymbol{r}')$ represents a product $\rho_1(\boldsymbol{r})\rho_a(\boldsymbol{r}')$ of two instantaneous density distributions in different replicas, or a statistical realization of density-density correlation function [62,63].
- To perform the configurational integral Tr_a in the second line on the rhs of Equation (16), it is indispensable to introduce the Fourier transform representation of the delta functional using the functional integral over the one-body potential field, which is dual to the density field $\rho_a(\boldsymbol{r})$ [84–88]. The ideal gas entropy given by Equation (17) appears in the last line of Equation (16) due to the saddle-point approximation of the one-body potential field [84–88].
- When different replica particles form complexes because of the attractive inter-replica interactions between them (i.e., $\widetilde{v}(\boldsymbol{r}) < 0$), we have $\widetilde{G}(\boldsymbol{r})/\overline{\rho}^2 \gg 1$ in an overlapped region (e.g., $|\boldsymbol{r}| \leq a$), thereby providing a significant value of overlap Q that is greater than the random overlap obtained from $\widetilde{G}(\boldsymbol{r}) = \overline{\rho}^2$. The glassy state preserves an overlapped state due to frozen configurations of particles even after the attractive inter-replica interactions are switched off (i.e., $\widetilde{v}(\boldsymbol{r}) \to 0$). The generalized FP potential $W(\widetilde{G})$ is available to explore such an overlapped state that is locally stable.
- It is also noted that the above formalism presented in Equations (10)–(17) has been conventionally used for the formulation of continuous field theory [79–88]; the density operator $\widehat{\rho}_b^{(N)}(\boldsymbol{r})$ ($b = 1$, a) has been mapped to a density field $\rho_b(\boldsymbol{r})$ using the density functional integral in Equations (13) and (16) according to the conventional formalism in statistical field theory [79] (see also the literature [80–91] for discussions about the underlying physics of this formal procedure to introduce a continuous density field).

3. Main Results

We present four sets of main results based on the strong-coupling perturbation theory (see Appendix B for details). Figure 1 summarizes the results schematically.

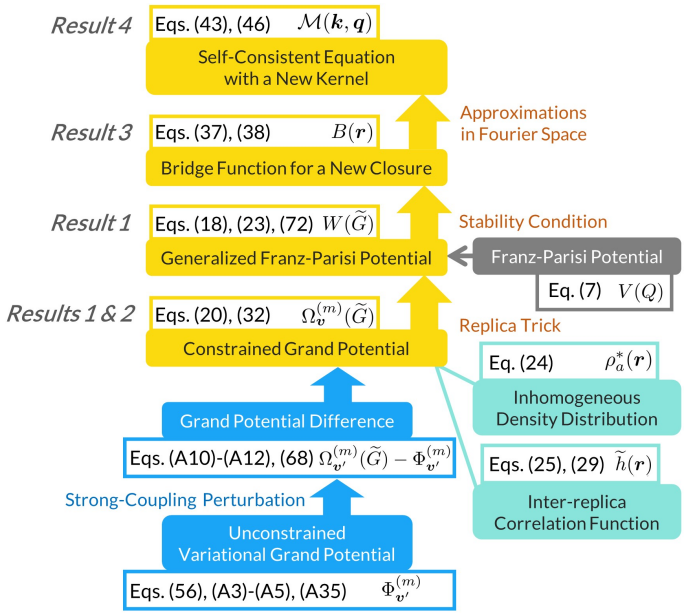

Figure 1. A schematic summary of the main results colored orange. In addition, functional variables are colored green, and underlying potentials blue or gray.

3.1. Result 1: Replica Formalism of the Generalized FP Potential

Let $\Omega_v^{(m)}(\widetilde{G})$ be the constrained grand potential of m replicas defined by

$$\begin{aligned} e^{-\beta\Omega_v^{(m)}(\widetilde{G})} &= \mathbf{Tr}\, e^{-\beta U(\boldsymbol{v},\widehat{\boldsymbol{\rho}})} \prod_{a=2}^{m} \Delta_a(\widetilde{G},\widehat{\boldsymbol{\rho}}) \\ &= \int D\boldsymbol{\rho}\, \mathbf{Tr}\, e^{-\beta U(\boldsymbol{v},\boldsymbol{\rho})} \prod_{b=1}^{m} \prod_{\{\boldsymbol{r}\}} \delta\left[\rho_b(\boldsymbol{r}) - \widehat{\rho}_b^{(N)}(\boldsymbol{r})\right] \prod_{a=2}^{m} \Delta_a(\widetilde{G},\rho) \end{aligned} \tag{20}$$

where $\int D\boldsymbol{\rho} \equiv \prod_{b=1}^{m} \int D\rho_b$, $\mathbf{Tr} \equiv \prod_{b=1}^{m} \mathrm{Tr}_b$, the matrix elements of $\boldsymbol{v}$ are $v_{ab}(\boldsymbol{r}) = 0$ $(a \neq b)$ and $v_{aa}(\boldsymbol{r}) = v(\boldsymbol{r})$, $\widehat{\boldsymbol{\rho}} = (\widehat{\rho}_1^{(N)}, \cdots, \widehat{\rho}_m^{(N)})^{\mathrm{T}}$, $\boldsymbol{\rho} = (\rho_1, \cdots, \rho_m)^{\mathrm{T}}$, and the interaction energy $U(\boldsymbol{v},\widehat{\boldsymbol{\rho}})$ in Equation (20) is given by

$$U(\boldsymbol{v},\widehat{\boldsymbol{\rho}}) = \frac{1}{2} \iint d\boldsymbol{r} d\boldsymbol{r}' \left\{ \widehat{\boldsymbol{\rho}}(\boldsymbol{r})^{\mathrm{T}} \boldsymbol{v}(\boldsymbol{r}-\boldsymbol{r}') \widehat{\boldsymbol{\rho}}(\boldsymbol{r}') - \sum_{b=1}^{m} \widehat{\rho}_b^{(N)}(\boldsymbol{r}) v(\boldsymbol{r}-\boldsymbol{r}') \delta(\boldsymbol{r}-\boldsymbol{r}') \right\}, \tag{21}$$

excluding the intra-replica self-energy. Incidentally, there are two methods to treat the density functional integral in Equation (20) [79–88], both of which will be utilized as seen from Equations (A13) and (A35).

It is readily seen from Equations (16) and (20) that the constrained grand potential $\Omega_v^{(m)}(\widetilde{G})$ is expressed using $W(\widetilde{G},\widehat{\rho}_1)$ as

$$e^{-\beta\Omega_v^{(m)}(\widetilde{G})} = \mathrm{Tr}_1\, e^{-\beta U_{\mathrm{intra}}(\widehat{\rho}_1) - (m-1)\beta N^* W(\widetilde{G},\widehat{\rho}_1)}. \tag{22}$$

The replica trick allows us to have the relation between the constrained grand potential $\Omega_v^{(m)}$ and the generalized FP potential $W(\widetilde{G})$:

$$N^* W(\widetilde{G}) = \lim_{m\to 1} \frac{\partial \Omega_v^{(m)}(\widetilde{G})}{\partial m}, \tag{23}$$

which is the first result (*Result 1*; see Appendix A for the detailed derivation). It is noted that the conventional replica trick proves the necessity of $m \to 1$ to consider the quenched type of the FP formalism, though it has been physically motivated to take the limit of $m \to 1$ based on the Monasson formalism [18,22,75].

3.2. Result 2: The Constrained Grand Potential Functional of m Replicas in an Inhomogeneous State

In *Result 2*, we provide the correlation functional form of the constrained grand potential $\Omega_v^{(m)}(\widetilde{G})$. Section 4 will sketch how the perturbative field theory developed in Appendix B yields the correlation functional given in *Result 2*.

Let us consider the inhomogeneous system characterized by the mean-field density $\rho_a^*(\boldsymbol{r})$ satisfying

$$\rho_a^*(\boldsymbol{r}) = e^{\beta\mu - \frac{c_{aa}(\boldsymbol{0})}{2}} \exp\left\{ \sum_{b=1}^{m} \int d\boldsymbol{r}' c_{ab}(\boldsymbol{r}-\boldsymbol{r}') \rho_b^*(\boldsymbol{r}') \right\}, \tag{24}$$

where $c_{ab}(\boldsymbol{r})$ denotes the two-point DCF (simply called DCF) between replica a and replica b. Here we suppose that a given function $\widetilde{G}(\boldsymbol{r},\boldsymbol{r}')$ imposed on the inter-replica correlation between replica 1 and replica a $(a \geq 2)$ is expressed as

$$\widetilde{G}(\boldsymbol{r},\boldsymbol{r}') = \rho_1^*(\boldsymbol{r}) \rho_a^*(\boldsymbol{r}')\, \widetilde{g}(\boldsymbol{r}-\boldsymbol{r}') = \rho_1^*(\boldsymbol{r}) \rho_a^*(\boldsymbol{r}') \left\{ 1 + \widetilde{h}(\boldsymbol{r}-\boldsymbol{r}') \right\}, \tag{25}$$

using a statistical realization of inter-replica radial distribution function $\widetilde{g}(\boldsymbol{r})$ or inter-replica total correlation function (TCF) $\widetilde{h}(\boldsymbol{r}) \equiv \widetilde{g}(\boldsymbol{r}) - 1$ [62,63]. Namely, Equations (14) and (25) imply the constraint,

$$\rho_1^*(\boldsymbol{r})\rho_a^*(\boldsymbol{r}')\left\{1 + \widetilde{h}(\boldsymbol{r}-\boldsymbol{r}')\right\} = \rho_1(\boldsymbol{r})\rho_a(\boldsymbol{r}'), \tag{26}$$

on $\rho_1(\boldsymbol{r})\rho_a(\boldsymbol{r}')$ which is a statistical realization of density-density correlation [62,63] as mentioned above. Equation (26) includes the trivial inter-replica constraints as follows: one constraint, $\overline{\rho}^2 = \rho_1(\boldsymbol{r})\rho_a(\boldsymbol{r}')$ (i.e., $\widetilde{h}(\boldsymbol{r}-\boldsymbol{r}') = 0$), forces the two-replica system to maintain uniformity without inter-replica correlations, whereas another constraint, $0 = \rho_1(\boldsymbol{r})\rho_a(\boldsymbol{r}')$ (i.e., $\widetilde{h}(\boldsymbol{r}-\boldsymbol{r}') = -1$), imposes a region where two particles of different replicas exclude each other. In Section 3.3, we will see that the metastable TCF $\widetilde{h}_*(\boldsymbol{r}-\boldsymbol{r}')$ corresponds to the TCF obtained from averaging over statistical realizations of instantaneous density-density correlation $\rho_1(\boldsymbol{r})\rho_a(\boldsymbol{r}')$ consistently with Equation (26) as well as the liquid-state theory [62,63].

Let $\boldsymbol{h}(\boldsymbol{r})$ and $\boldsymbol{c}(\boldsymbol{r})$ be the correlation matrices of TCFs and DCFs, respectively. The intra- and inter-replica matrix elements vary, depending on whether replica 1 is included or not: when setting $\boldsymbol{\chi}(\boldsymbol{r}) = \boldsymbol{h}(\boldsymbol{r})$ or $\boldsymbol{c}(\boldsymbol{r})$ with the subscripts of their matrix elements denoting a pair of replicas, $\chi_{11}(\boldsymbol{r}) = \chi_1(\boldsymbol{r})$ and $\chi_{aa}(\boldsymbol{r}) = \chi(\boldsymbol{r})$ for $a \geq 2$, whereas $\chi_{1a}(\boldsymbol{r}) = \chi_{a1}(\boldsymbol{r}) = \widetilde{\chi}(\boldsymbol{r})$ for $a \geq 2$ and $\chi_{ab}(\boldsymbol{r}) = \widetilde{\chi}'(\boldsymbol{r})$ for $a \neq b$ and $a, b \geq 2$. As a consequence, we see from Equation (24) that

$$\rho_1^*(\boldsymbol{r}) = e^{\beta\mu - \frac{c_1(\boldsymbol{0})}{2}} \exp\left\{\int d\boldsymbol{r}' c_1(\boldsymbol{r}-\boldsymbol{r}')\rho_1^*(\boldsymbol{r}') + (m-1)\int d\boldsymbol{r}'\widetilde{c}(\boldsymbol{r}-\boldsymbol{r}')\rho^*(\boldsymbol{r}')\right\}, \tag{27}$$

where $\rho_a^*(\boldsymbol{r}) = \rho^*(\boldsymbol{r})$ for $a \geq 2$. It is noted that the metastable density distribution $\rho_1^*(\boldsymbol{r})$ reduces to that from the Ramakrishnan-Yussouf density functional [58–61]:

$$\rho_1^*(\boldsymbol{r}) = e^{\beta\mu - \frac{c_1(\boldsymbol{0})}{2}} \exp\left\{\int d\boldsymbol{r}' c_1(\boldsymbol{r}-\boldsymbol{r}')\rho_1^*(\boldsymbol{r}')\right\}, \tag{28}$$

in the limit of $m \to 1$.

The variational approach presented in Appendix B.1 justifies the following set of inhomogeneous Ornstein-Zernike equations [33–38,62,63]: in general, we have

$$h_{ac}(\boldsymbol{r}-\boldsymbol{r}') = c_{ac}(\boldsymbol{r}-\boldsymbol{r}') + \sum_{b=1}^{m}\int d\boldsymbol{r}'\rho_b^*(\boldsymbol{r}'')c_{ab}(\boldsymbol{r}-\boldsymbol{r}'')h_{bc}(\boldsymbol{r}''-\boldsymbol{r}'), \tag{29}$$

which reads

$$\begin{aligned} h_1(\boldsymbol{r}-\boldsymbol{r}') = c_1(\boldsymbol{r}-\boldsymbol{r}') &+ \int d\boldsymbol{r}''\rho_1^*(\boldsymbol{r}'')c_1(\boldsymbol{r}-\boldsymbol{r}'')h_1(\boldsymbol{r}''-\boldsymbol{r}') \\ &+ (m-1)\int d\boldsymbol{r}''\rho^*(\boldsymbol{r}'')\widetilde{c}(\boldsymbol{r}-\boldsymbol{r}'')\widetilde{h}(\boldsymbol{r}''-\boldsymbol{r}'), \end{aligned} \tag{30}$$

and

$$\begin{aligned} \widetilde{h}(\boldsymbol{r}-\boldsymbol{r}') = \widetilde{c}(\boldsymbol{r}-\boldsymbol{r}') &+ \int d\boldsymbol{r}''\left\{\rho^*(\boldsymbol{r}'')\widetilde{c}(\boldsymbol{r}-\boldsymbol{r}'')h(\boldsymbol{r}''-\boldsymbol{r}') + \rho_1^*(\boldsymbol{r}'')c_1(\boldsymbol{r}-\boldsymbol{r}'')\widetilde{h}(\boldsymbol{r}''-\boldsymbol{r}')\right\} \\ &+ (m-2)\int d\boldsymbol{r}''\rho^*(\boldsymbol{r}'')\widetilde{c}(\boldsymbol{r}-\boldsymbol{r}'')\widetilde{h}(\boldsymbol{r}''-\boldsymbol{r}'), \end{aligned} \tag{31}$$

in agreement with previous expressions [33–38].

The second result (*Result 2*) can be obtained using the perturbative field theory at strong coupling (see Appendix B). It will be shown in Section 4 that the constrained grand potential is of the following functional form:

$$
\begin{aligned}
&\beta\Omega_{v'}^{(m)}(\widetilde{G}) \\
&\quad = \frac{1}{2}\iint d\boldsymbol{r}_0 d\boldsymbol{r}\,\{\rho_1^*(\boldsymbol{r}_0)\rho_1^*(\boldsymbol{r}_0-\boldsymbol{r}) + (m-1)\rho^*(\boldsymbol{r}_0)\rho^*(\boldsymbol{r}_0-\boldsymbol{r})\}g(\boldsymbol{r})v(\boldsymbol{r}) \\
&\quad + (m-1)\iint d\boldsymbol{r}_0 d\boldsymbol{r}\,\rho_1^*(\boldsymbol{r}_0)\rho^*(\boldsymbol{r}_0-\boldsymbol{r})\widetilde{g}(\boldsymbol{r})\widetilde{v}(\boldsymbol{r}) \\
&\quad + \int d\boldsymbol{r}_0\,[\rho_1^*(\boldsymbol{r}_0)\{\ln\rho_1^*(\boldsymbol{r}_0) - 1 - \beta\mu\} + (m-1)\rho^*(\boldsymbol{r}_0)\{\ln\rho^*(\boldsymbol{r}_0) - 1 - \beta\mu\}] \\
&\quad + \frac{1}{2}\iint d\boldsymbol{r}_0 d\boldsymbol{r}\,\{\rho_1^*(\boldsymbol{r}_0)h_1(\boldsymbol{r})\delta(\boldsymbol{r}) + (m-1)\rho^*(\boldsymbol{r}_0)h(\boldsymbol{r})\delta(\boldsymbol{r}) - \ln|\boldsymbol{S}|\} \\
&\quad + (m-1)\iint d\boldsymbol{r}_0 d\boldsymbol{r}\,\rho_1^*(\boldsymbol{r}_0)\rho^*(\boldsymbol{r}_0-\boldsymbol{r})\Big\{\widetilde{g}(\boldsymbol{r})\ln\widetilde{g}(\boldsymbol{r}) - \widetilde{h}(\boldsymbol{r}) - \widetilde{h}^2(\boldsymbol{r}) + e^{\widetilde{h}(\boldsymbol{r})} - \widetilde{g}(\boldsymbol{r})\Big\},
\end{aligned}
\tag{32}
$$

where the matrix elements of v' has a non-zero potential $v_{1a}(\boldsymbol{r}) = v_{a1}(\boldsymbol{r}) = \widetilde{v}(\boldsymbol{r})$ between replica 1 and replica a that enforces Equation (26) without the constraint $\Delta_a(\widetilde{G}, \widehat{\boldsymbol{\rho}})$, and the matrix element of $\boldsymbol{S}$ is given by $S_{ab}(\boldsymbol{r}) = \delta_{ab}\delta(\boldsymbol{r}) + \rho_a^*(\boldsymbol{r}_0)h_{ab}(\boldsymbol{r})$. It is noted that the last line of Equation (32) is reduced to the RHNC functional of $\widetilde{h}(\boldsymbol{r})$ in the approximation of $e^{\widetilde{h}(\boldsymbol{r})} - \widetilde{g}(\boldsymbol{r}) \approx \widetilde{h}^2(\boldsymbol{r})/2$ [33–38,62–64,85,92].

3.3. Result 3: New Closure Obtained from the Generalized FP Potential

The stationary condition of $W(\widetilde{G})$ given by Equation (23) can be written as

$$
\left.\frac{\delta W(\widetilde{G})}{\delta\widetilde{h}}\right|_{\widetilde{h}=\widetilde{h}_*} = \frac{1}{N^*}\lim_{\widetilde{v}\to 0}\frac{\delta}{\delta\widetilde{h}}\left\{\lim_{m\to 1}\frac{\partial\Omega_{v'}^{(m)}(\widetilde{G})}{\partial m}\right\}\Bigg|_{\widetilde{h}=\widetilde{h}_*} = 0. \tag{33}
$$

It is found from Equation (32) that

$$
\begin{aligned}
\lim_{m\to 1}\frac{\partial\beta\Omega_{v'}^{(m)}(\widetilde{G})}{\partial m} &= \iint d\boldsymbol{r}_0 d\boldsymbol{r}\left\{\frac{1}{2}\rho^*(\boldsymbol{r}_0)\rho^*(\boldsymbol{r}_0-\boldsymbol{r})g(\boldsymbol{r})v(\boldsymbol{r}) + \rho_1^*(\boldsymbol{r}_0)\rho^*(\boldsymbol{r}_0-\boldsymbol{r})\widetilde{g}(\boldsymbol{r})\widetilde{v}(\boldsymbol{r})\right\} \\
&\quad + \int d\boldsymbol{r}_0\,\rho^*(\boldsymbol{r}_0)\{\ln\rho^*(\boldsymbol{r}_0) - 1 - \beta\mu\} + \frac{1}{2}\iint d\boldsymbol{r}_0 d\boldsymbol{r}\,\rho^*(\boldsymbol{r}_0)h(\boldsymbol{r})\delta(\boldsymbol{r}) \\
&\quad + \frac{1}{2}\iint d\boldsymbol{r}_0 d\boldsymbol{r}\,\rho_1^*(\boldsymbol{r}_0)\rho^*(\boldsymbol{r}_0-\boldsymbol{r})\widetilde{c}(\boldsymbol{r})\widetilde{h}(\boldsymbol{r}) \\
&\quad + \iint d\boldsymbol{r}_0 d\boldsymbol{r}\,\rho_1^*(\boldsymbol{r}_0)\rho^*(\boldsymbol{r}_0-\boldsymbol{r})\Big\{\widetilde{g}(\boldsymbol{r})\ln\widetilde{g}(\boldsymbol{r}) - \widetilde{h}(\boldsymbol{r}) - \widetilde{h}^2(\boldsymbol{r}) + e^{\widetilde{h}(\boldsymbol{r})} - \widetilde{g}(\boldsymbol{r})\Big\},
\end{aligned}
\tag{34}
$$

where the third line of Equation (34) is obtained from the derivative of the logarithmic term in the fifth line of Equation (32) with respect to m using the Laplace expansion of $|\boldsymbol{S}|$ along the first row as follows:

$$
\begin{aligned}
-\frac{1}{2}\frac{\partial}{\partial m}\ln|\boldsymbol{S}(\boldsymbol{r})| &= -\frac{1}{2|\boldsymbol{S}(\boldsymbol{r})|}\left(\frac{\partial|\boldsymbol{S}(\boldsymbol{r})|}{\partial m}\right) \\
&= \frac{1}{2}\rho_1^*(\boldsymbol{r}_0)\rho^*(\boldsymbol{r}_0-\boldsymbol{r})\widetilde{c}(\boldsymbol{r})\widetilde{h}(\boldsymbol{r}),
\end{aligned}
\tag{35}
$$

where use has been made of the cofactor expansion in calculating $\partial|\boldsymbol{S}(\boldsymbol{r})|/\partial m$.

It follows from Equation (34) that the stationary condition (33) becomes

$$
\left.\frac{\delta W(\widetilde{G})}{\delta\widetilde{h}}\right|_{\widetilde{h}=\widetilde{h}_*} \approx \frac{1}{N^*}\int d\boldsymbol{r}_0\,\rho^*(\boldsymbol{r}_0)\rho^*(\boldsymbol{r}_0-\boldsymbol{r})\Big\{\widetilde{c}_*(\boldsymbol{r}) + \ln\widetilde{g}_*(\boldsymbol{r}) - 1 - 2\widetilde{h}_*(\boldsymbol{r}) + e^{\widetilde{h}_*(\boldsymbol{r})}\Big\} = 0, \tag{36}
$$

where the subscript 1 has been dropped because of the indistinguishability of all replicas in the limits of $m \to 1$ and $\widetilde{v}(\boldsymbol{r}) \to 0$, $\delta\widetilde{h}/\delta\rho^*$ and its inverse are ignored, and the first term on the rhs is an approximate form obtained from the third line of Equation (34) (see

Appendix F for the detailed derivation). We can easily verify the equivalence between Equation (36) and the following closure:

$$\widetilde{g}_*(\boldsymbol{r}) = e^{\widetilde{h}_*(\boldsymbol{r})-\widetilde{c}_*(\boldsymbol{r})+B(\boldsymbol{r})}, \tag{37}$$

$$B(\boldsymbol{r}) = \widetilde{g}_*(\boldsymbol{r}) - e^{\widetilde{h}_*(\boldsymbol{r})}, \tag{38}$$

which corresponds to the third result (*Result 3*), a new closure in the context of the liquid-state theory [62,63].

Two remarks on Equations (33), (37) and (38) are in order:

- Equation (33) is valid when a metastable state at $\widetilde{h}_*(\boldsymbol{r}) = \widetilde{h}(\boldsymbol{r})$ is stable in the vanishing limit of the inter-replica interaction potential (i.e., $\widetilde{v}(\boldsymbol{r}) \to 0$); otherwise, transitions between basins occur in the FEL and the inter-replica correlations disappear, thereby amounting to $\widetilde{g}_*(\boldsymbol{r}) = 1 + \widetilde{h}_*(\boldsymbol{r}) = 1$, the trivial solution to Equation (33). In other words, the new closure (37) applies to the metastable state defined by Equation (33).
- The bridge function $B(\boldsymbol{r})$ given by Equation (38) is approximated by $B(\boldsymbol{r}) = -\widetilde{h}_*^2(\boldsymbol{r})/2$, which coincides with the main term of either the soft mean spherical approximation (MSA) or various approximations used for hard-sphere systems [63,85].

3.4. Result 4: Self-Consistent Equation for the Non-Ergodicity Parameter

In the fourth result (*Result 4*), we restrict ourselves to uniform systems in Fourier space. We introduce the non-ergodicity parameter $f(\boldsymbol{k})$ by relating the inter-replica TCF $\widetilde{h}_*(\boldsymbol{k})$ to the intra-replica structure factor $S(\boldsymbol{k}) = 1 + \overline{\rho}h_*(\boldsymbol{k})$ [15,16,33–38]:

$$f(\boldsymbol{k}) = \frac{\overline{\rho}\widetilde{h}_*(\boldsymbol{k})}{S(\boldsymbol{k})}. \tag{39}$$

We need to find an approximation of the closure (37) that is available to obtain the self-consistent equation including terms up to quadratic order in the non-ergodicity parameter $f(\boldsymbol{k})$. It is appropriate for this purpose to expand the rhs of the closure (37), providing

$$\widetilde{g}_*(\boldsymbol{r}) \approx \widetilde{g}_*(\boldsymbol{r}) - \widetilde{c}_*(\boldsymbol{r}) + B(\boldsymbol{r}) + \frac{1}{2}\Big\{\widetilde{h}_*(\boldsymbol{r}) - \widetilde{c}_*(\boldsymbol{r})\Big\}^2. \tag{40}$$

Equation (40) reads in Fourier space

$$\widetilde{c}_*(\boldsymbol{k}) = \frac{1}{2}\int d\boldsymbol{q}\,\Big\{\widetilde{c}_*(\boldsymbol{q})\,\widetilde{c}_*(\boldsymbol{k}-\boldsymbol{q}) - \widetilde{c}_*(\boldsymbol{q})\,\widetilde{h}_*(\boldsymbol{k}-\boldsymbol{q}) - \widetilde{h}_*(\boldsymbol{q})\,\widetilde{c}_*(\boldsymbol{k}-\boldsymbol{q})\Big\}, \tag{41}$$

when making the approximation of $B(\boldsymbol{r}) \approx -h_*^2(\boldsymbol{r})/2$ as remarked after Equation (38). Meanwhile, the neglect of inhomogeneity (i.e., $\rho^*(\boldsymbol{r}) = \overline{\rho}$) allows us to express the Fourier transform of the Ornstein-Zernike Equation (31) at $m = 1$ as

$$\widetilde{c}_*(\boldsymbol{k}) = \frac{1}{\overline{\rho}S(\boldsymbol{k})}\left\{\frac{f(\boldsymbol{k})}{1-f(\boldsymbol{k})}\right\}, \tag{42}$$

using the non-ergodicity parameter $f(\boldsymbol{k})$ defined by Equation (39).

Combining Equations (39), (41) and (42), we obtain the self-consistent equation for $f(\boldsymbol{k})$ (*Result 4*):

$$\frac{f(\boldsymbol{k})}{1-f(\boldsymbol{k})} = \frac{S(\boldsymbol{k})}{2\overline{\rho}}\int d\boldsymbol{q}\,\mathcal{M}(\boldsymbol{k},\boldsymbol{q})\,S(\boldsymbol{q})\,S(\boldsymbol{k}-\boldsymbol{q})\,f(\boldsymbol{q})\,f(\boldsymbol{k}-\boldsymbol{q}) + \mathcal{O}[f^3], \tag{43}$$

where the inverse of the intra-replica structure factor $S(\boldsymbol{q})$ is related to the intra-replica DCF $c_*(\boldsymbol{q})$ as $1/S(\boldsymbol{q}) = 1 - \overline{\rho} c_*(\boldsymbol{q})$ and the kernel $\mathcal{M}(\boldsymbol{k}, \boldsymbol{q})$ is given by

$$\begin{aligned}\mathcal{M}(\boldsymbol{k}, \boldsymbol{q}) &= \frac{1}{S^2(\boldsymbol{q})\, S^2(\boldsymbol{k}-\boldsymbol{q})} - \frac{1}{S^2(\boldsymbol{q})} - \frac{1}{S^2(\boldsymbol{k}-\boldsymbol{q})} \\ &= \left\{\overline{\rho}^2 c_*(\boldsymbol{q})\, c_*(\boldsymbol{k}-\boldsymbol{q})\right\}^2 + 2\overline{\rho}^2 c_*(\boldsymbol{q})\, c_*(\boldsymbol{k}-\boldsymbol{q})\left\{\frac{1}{S(\boldsymbol{q})} + \frac{1}{S(\boldsymbol{k}-\boldsymbol{q})}\right\} - 1; \end{aligned} \tag{44}$$

see Appendix G for details. We can relate the product $c_*(\boldsymbol{q})\, c_*(\boldsymbol{k}-\boldsymbol{q})$ in Equation (44) to the triplet DCF $c_*^{(3)}(\boldsymbol{q}, \boldsymbol{k}-\boldsymbol{q})$ by adopting the approximate form as follows:

$$c_*^{(3)}(\boldsymbol{q}, \boldsymbol{k}-\boldsymbol{q}) = \frac{c_*^{(3)}(\boldsymbol{0}, \boldsymbol{0})}{\{c_*(\boldsymbol{0})\}^2}\, c_*(\boldsymbol{q})\, c_*(\boldsymbol{k}-\boldsymbol{q}), \tag{45}$$

which is validated by the weighted density approximation or the closure-based density functional theory [76–78]. The expression (45) and the introduction of the negative factor, $\alpha = \{c_*(\boldsymbol{0})\}^2 / c_*^{(3)}(\boldsymbol{0}, \boldsymbol{0}) < 0$, transform Equation (44) into the following kernel (*Result 4*):

$$\mathcal{M}(\boldsymbol{k}, \boldsymbol{q}) = \left\{\overline{\rho}^2 \alpha c_*^{(3)}(\boldsymbol{q}, \boldsymbol{k}-\boldsymbol{q})\right\}^2 + 2\overline{\rho}^2 \alpha c_*^{(3)}(\boldsymbol{q}, \boldsymbol{k}-\boldsymbol{q})\left\{\frac{1}{S(\boldsymbol{q})} + \frac{1}{S(\boldsymbol{k}-\boldsymbol{q})}\right\} - 1, \tag{46}$$

where $\alpha = \{c_*(\boldsymbol{0})\}^2 / c_*^{(3)}(\boldsymbol{0}, \boldsymbol{0})$ and $c_*^{(3)}(\boldsymbol{q}, \boldsymbol{k}-\boldsymbol{q})$ denotes the triplet DCF [76–78]. It is noted that Equation (46) can be compared with the previous result from other static theories [37,56,57]: the systematic expansion methods lead to the appearance of the triplet DCF in the kernel [37,56,57], similar to Equation (46).

4. Derivation Process of *Result 2*

This section presents a scheme to obtain *Result 2* based on the strong-coupling perturbation theory (see Appendix B). To this end, we focus on how to perform the functional integrals over one-body and two-body potential fields appearing in Equations (A12), (A20), (A29) and (A32)–(A34).

4.1. One-Body Potential Field (1): Evaluating Equation (A32) in the Saddle-Point Approximation

We see from Equation (A31) that the saddle-point equation $\delta \mathcal{H}_{\mathrm{mf}}(\boldsymbol{\phi})/\delta\phi|_{\phi_a = i\psi_a^*} = 0$ in Equation (A32) gives

$$\left.\frac{\delta \beta \mathcal{H}_0(\boldsymbol{c}, \boldsymbol{\phi})}{\delta \phi_a}\right|_{\phi_a = i\psi_a^*} = \left(\frac{\overline{\rho}}{\gamma}\right) \left.\frac{\delta \mathcal{U}_1(\boldsymbol{\phi})}{\delta \phi_a}\right|_{\phi_a = i\psi_a^*}. \tag{47}$$

Substituting Equations (A15) and (A26) into Equation (47), we have

$$\psi_a^*(\boldsymbol{r}) = \frac{c_{aa}(\boldsymbol{0})}{2} - e^{\beta\mu} \sum_{b=1}^{m} \int d\boldsymbol{r}' c_{ab}(\boldsymbol{r}-\boldsymbol{r}') e^{-\psi_b^*(\boldsymbol{r}')}. \tag{48}$$

We can verify that Equation (48) transforms to Equation (24) by setting $\rho_a^*(\boldsymbol{r}) = e^{\beta\mu - \psi_a^*(\boldsymbol{r})}$.

Let $F_{\mathrm{mf}}(-k_B T \boldsymbol{c}, \boldsymbol{\rho}^*)$ be the mean-field free energy defined by

$$F_{\mathrm{mf}}(-k_B T \boldsymbol{c}, \boldsymbol{\rho}^*) = U(-k_B T \boldsymbol{c}, \boldsymbol{\rho}^*) - T \mathcal{S}^{\mathrm{id}}(\boldsymbol{\rho}^*), \tag{49}$$

where $U(\boldsymbol{v}, \widehat{\boldsymbol{\rho}})$ has been defined in Equation (21) and $\mathcal{S}^{\mathrm{id}}(\boldsymbol{\rho}^*)$ denotes the sum of ideal gas entropy $\mathcal{S}_a^{\mathrm{id}}(\rho_a^*)$ given by Equation (17):

$$-T\mathcal{S}^{\mathrm{id}}(\boldsymbol{\rho}^*) = -T\sum_{a=1}^{m}\mathcal{S}_a^{\mathrm{id}}(\rho_a^*)$$
$$= k_BT\int d\boldsymbol{r}_0\,[\,\rho_1^*(\boldsymbol{r}_0)\{\ln\rho_1^*(\boldsymbol{r}_0)-1-\beta\mu\}+(m-1)\rho^*(\boldsymbol{r}_0)\{\ln\rho^*(\boldsymbol{r}_0)-1-\beta\mu\}]. \quad (50)$$

Plugging Equation (24) into Equations (49) and (50), we find

$$\beta F_{\mathrm{mf}}(-k_BT\boldsymbol{c},\boldsymbol{\rho}^*) = \frac{1}{2}\iint d\boldsymbol{r}d\boldsymbol{r}'\boldsymbol{\rho}^*(\boldsymbol{r})^{\mathrm{T}}\boldsymbol{c}(\boldsymbol{r}-\boldsymbol{r}')\boldsymbol{\rho}^*(\boldsymbol{r}') - \sum_{a=1}^{m}\int d\boldsymbol{r}\,\rho_a^*(\boldsymbol{r})$$
$$= \beta\mathcal{H}_{\mathrm{mf}}(i\boldsymbol{\psi}^*) \quad (51)$$

(see also Appendix C for details of the last equality).

The quadratic terms due to fluctuations around the saddle-point path $i\boldsymbol{\psi}^*$ are written as

$$\beta\mathcal{H}_{\mathrm{mf}}(\boldsymbol{\varphi}+i\boldsymbol{\psi}^*) - \beta\mathcal{H}_{\mathrm{mf}}(i\boldsymbol{\psi}^*)$$
$$\approx -\frac{1}{2}\iint d\boldsymbol{r}d\boldsymbol{r}'\boldsymbol{\varphi}^{\mathrm{T}}(\boldsymbol{r})\boldsymbol{c}^{-1}(\boldsymbol{r}-\boldsymbol{r}')\boldsymbol{\varphi}(\boldsymbol{r}') + \sum_{a=1}^{m}\frac{1}{2}\int d\boldsymbol{r}\rho_a^*(\boldsymbol{r})\varphi_a^2(\boldsymbol{r})$$
$$= -\frac{1}{2}\iint d\boldsymbol{r}d\boldsymbol{r}'\boldsymbol{\varphi}(\boldsymbol{r})^{\mathrm{T}}\boldsymbol{h}^{-1}(\boldsymbol{r}-\boldsymbol{r}')\boldsymbol{\varphi}(\boldsymbol{r}'). \quad (52)$$

In the last equality of Equation (52), use has been made of the following relation:

$$h_{ab}^{-1}(\boldsymbol{r}-\boldsymbol{r}') = c_{ab}^{-1}(\boldsymbol{r}-\boldsymbol{r}') - \rho_a^*(\boldsymbol{r})\delta_{ab}\delta(\boldsymbol{r}-\boldsymbol{r}'), \quad (53)$$

which is equivalent to the inhomogeneous Ornstein-Zernike Equations (29) as confirmed in Appendix D. It is found from Equations (51) and (52) that the saddle-point approximation of Equation (A32) yields

$$e^{-\beta\mathcal{F}(\boldsymbol{\nu}=\boldsymbol{0})} = \frac{1}{\mathcal{N}_c}\,e^{-\beta F_{\mathrm{mf}}(-k_BT\boldsymbol{c},\boldsymbol{\rho}^*)}\int D\boldsymbol{\varphi}\,e^{\frac{1}{2}\iint d\boldsymbol{r}d\boldsymbol{r}'\boldsymbol{\varphi}(\boldsymbol{r})^{\mathrm{T}}\boldsymbol{h}^{-1}(\boldsymbol{r}-\boldsymbol{r}')\boldsymbol{\varphi}(\boldsymbol{r}')}. \quad (54)$$

Equations (A14)–(A16) further imply that Equation (54) is transformed into

$$e^{-\beta\mathcal{F}(\boldsymbol{\nu}=\boldsymbol{0})} = \frac{\mathcal{N}_h}{\mathcal{N}_c}\,e^{-\beta F_{\mathrm{mf}}(-k_BT\boldsymbol{c},\boldsymbol{\rho}^*)}$$
$$= \frac{1}{\mathcal{N}_c}\,e^{-\beta F_{\mathrm{mf}}(-k_BT\boldsymbol{c},\boldsymbol{\rho}^*)}\int D\boldsymbol{\varphi}\,e^{-\beta\mathcal{H}_0(\boldsymbol{h},\boldsymbol{\varphi})}. \quad (55)$$

We will use the last line on the rhs of Equation (55) as a reference form in evaluating $\beta\mathcal{F}(\boldsymbol{\nu}) - \beta\mathcal{F}(\boldsymbol{\nu}=\boldsymbol{0})$ given by Equation (A33).

It follows from Equations (A32) and (55) that

$$\beta\Phi^{(m)}_{-k_BT\boldsymbol{c}} = \beta F_{\mathrm{mf}}(-k_BT\boldsymbol{c},\boldsymbol{\rho}^*) - \ln\frac{\mathcal{N}_h}{\mathcal{N}_c}, \quad (56)$$

where $\mathcal{N}_h/\mathcal{N}_c$ is related to the determinant of the matrix, $\boldsymbol{S} = \boldsymbol{c}^{-1}\boldsymbol{h}$, as

$$\frac{\mathcal{N}_h}{\mathcal{N}_c} = \left\{\prod_{\boldsymbol{r},\boldsymbol{r}'}|\boldsymbol{S}(\boldsymbol{r}-\boldsymbol{r}')|\right\}^{1/2}, \quad (57)$$

and the matrix element of $\boldsymbol{S}$ is given by

$$
\begin{aligned}
S_{ac}(\boldsymbol{r}-\boldsymbol{r}') &\equiv \sum_{b=1}^{m}\int d\boldsymbol{r}''\, c_{ab}^{-1}(\boldsymbol{r}-\boldsymbol{r}'')h_{bc}(\boldsymbol{r}''-\boldsymbol{r}') \\
&= \sum_{b=1}^{m}\int d\boldsymbol{r}''\left\{c_{ab}^{-1}(\boldsymbol{r}-\boldsymbol{r}'')c_{bc}(\boldsymbol{r}''-\boldsymbol{r}') + \sum_{d=1}^{m}\int d\boldsymbol{u}\,\rho_d^*(\boldsymbol{u})c_{ab}^{-1}(\boldsymbol{r}-\boldsymbol{r}'')c_{bd}(\boldsymbol{r}''-\boldsymbol{u})h_{dc}(\boldsymbol{u}-\boldsymbol{r}')\right\} \\
&= \delta_{ac}\delta(\boldsymbol{r}-\boldsymbol{r}') + \sum_{d=1}^{m}\int d\boldsymbol{u}\,\rho_d^*(\boldsymbol{u})\delta_{ad}\delta(\boldsymbol{r}-\boldsymbol{u})h_{dc}(\boldsymbol{u}-\boldsymbol{r}') \\
&= \delta_{ac}\delta(\boldsymbol{r}-\boldsymbol{r}') + \rho_a^*(\boldsymbol{r})h_{ac}(\boldsymbol{r}-\boldsymbol{r}') \\
&= \frac{\langle\rho_a(\boldsymbol{r})\rho_c(\boldsymbol{r}')\rangle}{\rho_c^*(\boldsymbol{r}')} \geq 0,
\end{aligned}
\tag{58}
$$

ensuring that $|\boldsymbol{S}| = |\boldsymbol{c}^{-1}\boldsymbol{h}| \geq 0$. Replacing $\boldsymbol{r}$ and $\boldsymbol{r}'$ by $\boldsymbol{r}_0$ and $\boldsymbol{r}_0 - \boldsymbol{r}$, respectively, in Equation (58), we have

$$
-\ln\frac{\mathcal{N}_h}{\mathcal{N}_c} = -\frac{1}{2}\iint d\boldsymbol{r}_0 d\boldsymbol{r}\,\ln|\boldsymbol{S}|, \tag{59}
$$

in agreement with the logarithmic term in Equation (32).

4.2. One-Body Potential Field (2): Perturbative Calculation of Equation (A12)

Remembering that $\rho_a^*(\boldsymbol{r}) = e^{\beta\mu-\psi_a^*(\boldsymbol{r})}$, the average term in Equation (A33) becomes

$$
\begin{aligned}
&\left(\frac{\overline{\rho}}{\gamma}\right)^2\left\langle e^{\int d\boldsymbol{r}\left\{i\phi_1(\boldsymbol{r})\widehat{\rho}_1^{(1)}(\boldsymbol{r})+i\phi_a(\boldsymbol{r})\widehat{\rho}_a^{(1)}(\boldsymbol{r})\right\}}\right\rangle_{\phi} \\
&\quad= \rho_1^*(\boldsymbol{r}_{1,1})\rho^*(\boldsymbol{r}_{a,1})\left\langle e^{\int d\boldsymbol{r}\left\{i\varphi_1(\boldsymbol{r})\widehat{\rho}_1^{(1)}(\boldsymbol{r})+i\varphi_a(\boldsymbol{r})\widehat{\rho}_a^{(1)}(\boldsymbol{r})\right\}}\right\rangle_{\varphi} \\
&\quad= \rho_1^*(\boldsymbol{r}_{1,1})\rho^*(\boldsymbol{r}_{a,1})\,e^{\widetilde{h}(\boldsymbol{r}_{1,1}-\boldsymbol{r}_{a,1})},
\end{aligned}
\tag{60}
$$

where the subscript φ denotes the following average:

$$
\langle\mathcal{O}\rangle_{\varphi} = \frac{\int D\boldsymbol{\varphi}\,\mathcal{O}\,e^{-\beta\mathcal{H}_0(\boldsymbol{h},\boldsymbol{\varphi})}}{\int D\boldsymbol{\varphi}\,e^{-\beta\mathcal{H}_0(\boldsymbol{h},\varphi)}}, \tag{61}
$$

according to Equation (55) (see Appendix E for the detailed derivation of Equation (60)).

It is noted that the one-particle densities, $\widehat{\rho}_1^{(1)}(\boldsymbol{r})$ and $\widehat{\rho}_a^{(1)}(\boldsymbol{r})$, of replicas 1 and a in Equation (60) represent the two-particle system as a mixture of two replicas. Accordingly, the last line on the rhs of Equation (60) reduces to $\rho^*(\boldsymbol{r}_{a,1})\rho_1^*(\boldsymbol{r}_{1,1})$ in the absence of inter-replica correlation between two particles of different replicas (i.e., $\widetilde{h}(\boldsymbol{r}_{a,1}-\boldsymbol{r}_{1,1}) = 0$) consistently with the following result for the sum of one-particle systems:

$$
\left\langle\frac{\overline{\rho}}{\gamma}\mathcal{U}_1(\boldsymbol{\phi})\right\rangle_{\phi} = \sum_{a=1}^{m}\int d\boldsymbol{r}_{a,1}\,\rho_a^*(\boldsymbol{r}_{a,1})\left\langle e^{\int d\boldsymbol{r}\,i\varphi_a(\boldsymbol{r})\widehat{\rho}_a^{(1)}(\boldsymbol{r})}\right\rangle_{\varphi} = \sum_{a=1}^{m}\int d\boldsymbol{r}_{a,1}\,\rho_a^*(\boldsymbol{r}_{a,1}), \tag{62}
$$

where the above φ-averaging is applied to the one-particle term $\mathcal{U}_1(\boldsymbol{\phi})$ given by Equation (A26), or setting $\mathcal{O} = (\overline{\rho}/\gamma)\,\mathcal{U}_1(\boldsymbol{\varphi}+i\boldsymbol{\psi}^*)$ in Equation (61) because of $\boldsymbol{\phi} = \boldsymbol{\varphi}+i\boldsymbol{\psi}^*$.

Combining Equations (A10), (A11), (A20), (A33) and (60), we obtain the additional contribution to $\beta\Phi_{v'}^{(m)}$ given by Equations (A5), (49), (56) and (59):

$$
\begin{aligned}
e^{-\beta\Omega_{v'}^{(m)}(\widetilde{G})+\beta\Phi_{v'}^{(m)}} &= \left\langle\prod_{a=2}^{m}\Delta_a(\widetilde{G},\rho)\right\rangle_{\boldsymbol{c}} \\
&= \int D'\boldsymbol{\nu}\,e^{-\sum_{a=2}^{m}\Gamma_a(\boldsymbol{\nu})},
\end{aligned}
\tag{63}
$$

and

$$\Gamma_a(\boldsymbol{\nu}) = -\iint d\boldsymbol{r}d\boldsymbol{r}'\,\rho_1^*(\boldsymbol{r})\rho^*(\boldsymbol{r}')\Big\{i\,\widetilde{g}(\boldsymbol{r}-\boldsymbol{r}')\,\nu_a(\boldsymbol{r}-\boldsymbol{r}') + e^{\widetilde{h}(\boldsymbol{r}-\boldsymbol{r}')}\,f(i\,\nu_a)\Big\}; \tag{64}$$

see Equation (A10) for the definition of $\langle\mathcal{O}\rangle_{\boldsymbol{c}}$. The results from the strong-coupling perturbation method developed in Appendix B are summed up in Equations (63) and (64).

4.3. Two-Body Potential Field: Derivation of Result 2: Rearrangements in the Mean-Field Approximation of Equation (63)

There are two remaining steps toward obtaining Equation (32): the first step is to evaluate the $\boldsymbol{\nu}$-functional integral given by Equation (63), and the second step is to rearrange the interaction energy when adding the last two terms on the rhs of Equation (A5) to $U(-k_BT\boldsymbol{c},\boldsymbol{\rho}^*)$.

First, let us evaluate the $\boldsymbol{\nu}$–field integral given by Equation (63) in the mean-field approximation. Equations (63) and (64) provide the saddle-point equation as follows:

$$\left.\frac{\delta\Gamma_a(\boldsymbol{\nu})}{\delta\nu_a}\right|_{\nu_a^*=iu} = 0, \tag{65}$$

giving

$$\widetilde{g}(\boldsymbol{r}) = e^{\widetilde{h}(\boldsymbol{r})+u(\boldsymbol{r})}, \tag{66}$$

similar to a closure in the liquid-state theory [62,63] though given correlation functions do not necessarily satisfy any closure, other than the Ornstein-Zernike equation. Substituting Equation (66) into Equation (64), we obtain

$$\Gamma_a(\boldsymbol{\nu}^*) = \iint d\boldsymbol{r}_0d\boldsymbol{r}\,\rho_1^*(\boldsymbol{r}_0)\rho^*(\boldsymbol{r}_0-\boldsymbol{r})\Big[\widetilde{g}(\boldsymbol{r})\Big\{\ln\widetilde{g}(\boldsymbol{r})-\widetilde{h}(\boldsymbol{r})\Big\}+e^{\widetilde{h}(\boldsymbol{r})}-\widetilde{g}(\boldsymbol{r})\Big], \tag{67}$$

or

$$\begin{aligned}&\Omega_{v'}^{(m)}(\widetilde{G})-\Phi_{v'}^{(m)}\\ &\quad=(m-1)\iint d\boldsymbol{r}_0d\boldsymbol{r}\,\rho_1^*(\boldsymbol{r}_0)\rho^*(\boldsymbol{r}_0-\boldsymbol{r})\Big[\widetilde{g}(\boldsymbol{r})\Big\{\ln\widetilde{g}(\boldsymbol{r})-\widetilde{h}(\boldsymbol{r})\Big\}+e^{\widetilde{h}(\boldsymbol{r})}-\widetilde{g}(\boldsymbol{r})\Big],\end{aligned} \tag{68}$$

due to Equations (63) and (64).

Next, we rewrite the interaction energy. Considering the expression (21) and the Ornstein-Zernike equation,

$$h_{aa}(\boldsymbol{0}) = c_{aa}(\boldsymbol{0}) + \sum_{b=1}^{m}\int d\boldsymbol{r}'\rho_b^*(\boldsymbol{r}')h_{ab}(\boldsymbol{r}-\boldsymbol{r}')c_{ab}(\boldsymbol{r}-\boldsymbol{r}'), \tag{69}$$

we have

$$\begin{aligned}U(-k_BT\boldsymbol{c},\boldsymbol{\rho}^*) &+ \sum_{a=1}^{m}\sum_{b=1}^{m}\frac{1}{2}\iint d\boldsymbol{r}d\boldsymbol{r}'\rho_a^*(\boldsymbol{r})\rho_b^*(\boldsymbol{r}')g_{ab}(\boldsymbol{r}-\boldsymbol{r}')c_{ab}(\boldsymbol{r}-\boldsymbol{r}')\\ &=\frac{1}{2}\sum_{a=1}^{m}\iint d\boldsymbol{r}_0d\boldsymbol{r}\,\rho_a^*(\boldsymbol{r}_0)h_{aa}(\boldsymbol{r})\delta(\boldsymbol{r})\\ &=\frac{1}{2}\iint d\boldsymbol{r}_0d\boldsymbol{r}\,\{\rho_1^*(\boldsymbol{r}_0)h_1(\boldsymbol{r})\delta(\boldsymbol{r})+(m-1)\rho^*(\boldsymbol{r}_0)h(\boldsymbol{r})\delta(\boldsymbol{r})\}.\end{aligned} \tag{70}$$

To clarify the difference between the bare interaction potentials of v and v', we also separate the intra-replica interaction term from the inter-replica one created by $\widetilde{v}(\boldsymbol{r}) = v_{a1}(\boldsymbol{r}) = v_{1a}(\boldsymbol{r})$:

$$\begin{aligned}\sum_{a=1}^{m}\sum_{b=1}^{m}\frac{1}{2}\iint d\boldsymbol{r}_0 d\boldsymbol{r}\rho_a^*(\boldsymbol{r})\rho_b^*(\boldsymbol{r}')g_{ab}(\boldsymbol{r}-\boldsymbol{r}')v_{ab}(\boldsymbol{r}-\boldsymbol{r}')&\\ =\frac{1}{2}\iint d\boldsymbol{r}_0 d\boldsymbol{r}\left\{\rho_1^*(\boldsymbol{r}_0)\rho_1^*(\boldsymbol{r}_0-\boldsymbol{r})+(m-1)\rho^*(\boldsymbol{r}_0)\rho^*(\boldsymbol{r}_0-\boldsymbol{r})\right\}g(\boldsymbol{r})v(\boldsymbol{r})&\\ +(m-1)\iint d\boldsymbol{r}_0 d\boldsymbol{r}\,\rho_1^*(\boldsymbol{r}_0)\rho^*(\boldsymbol{r}_0-\boldsymbol{r})\widetilde{g}(\boldsymbol{r})\widetilde{v}(\boldsymbol{r}).&\end{aligned} \tag{71}$$

Combining Equations (49), (50), (56), (59), (68), (70) and (71), we obtain $\beta\Omega_{v'}^{(m)}(\widetilde{G})$ expressed by Equation (32), namely *Result 2*.

5. Concluding Remarks

The generalized FP potential $W(\widetilde{G})$ as a functional of given TCF $\widetilde{h}(\boldsymbol{r})$ is similar to the original FP potential [65–75] in that both have constraints on inter-replica correlations. The difference is that the generalized FP potential adopts a local order parameter instead of a global order one, the overlap Q (see Equation (1)), used in the original FP potential $V(Q)$. Upon reviewing the formulation of $W(\widetilde{G})$ presented so far, we find two essentials for the field-theoretical achievements. The former lies in the variational method described in Appendix B.1, whereas Equation (A10) represents the latter. The details follow:

- *Unconstrained grand potential mimicking inter-replica correlations*: At first, we consider a coupled m-replica system that reproduces a given distribution of the inter-replica TCF $\widetilde{h}(\boldsymbol{r})$ without constraints. We tune the inter-replica interaction potential $\widetilde{v}(\boldsymbol{r})$ to mimic the inter-replica correlations. From evaluating the free-energy functional without constraints in the Gaussian approximation, we obtain the same functional form as the random phase approximation (RPA) in terms of the liquid-state theory [62,63]; however, the density distribution is different. The variational method presented in Appendix B.1 justifies the input of the density distribution given by Equation (27), which converges to that of the Ramakrishnan–Yussouf density functional theory [61] in the limit of $m \to 1$ as demonstrated in Equation (28).
- *Evaluating the difference between the constrained and unconstrained grand potentials*: Next, we take the free-energy functional of the unconstrained system as a reference energy. Equation (A10) indicates that the field-theoretical formulation focuses on the free energy difference between the constrained and unconstrained free-energy functionals. The strong-coupling expansion method developed in Appendix B.3 allows us to evaluate this difference in Sections 4.2 and 4.3. Thus, we obtain Equation (68), the constraint-associated free energy difference as a functional of inter-replica TCF $\widetilde{h}(\boldsymbol{r})$ and density distribution $\rho^*(\boldsymbol{r})$ determined by the Ramakrishnan-Yussouf theory [61].

Equation (68) reduces to the functional difference between the $\widetilde{h}(\boldsymbol{r})$-dependent parts in the HNC and RPA approximations when substituting $e^{\widetilde{h}(\boldsymbol{r})} - \widetilde{g}(\boldsymbol{r}) \approx \widetilde{h}^2(\boldsymbol{r})/2$ into Equation (68). This agreement indicates consistency between the field-theoretical formalism in this paper and the Legendre-transform-based theory using the Morita-Hiroike functional [33–38,64].

Combination of Equations (23) and (34) gives the difference between the generalized FP potentials at zero and a finite value of the inter-replica TCFs as follows:

$$\begin{aligned}W\left(\widetilde{G}=\overline{\rho}^2\left\{1+\widetilde{h}\right\}\right)-W(\overline{\rho}^2)&\\ =\frac{1}{2N^*}\iint d\boldsymbol{r}_0 d\boldsymbol{r}\,\rho^*(\boldsymbol{r}_0)\rho^*(\boldsymbol{r}_0-\boldsymbol{r})\widetilde{c}(\boldsymbol{r})\widetilde{h}(\boldsymbol{r})&\\ +\frac{1}{N^*}\iint d\boldsymbol{r}_0 d\boldsymbol{r}\,\rho^*(\boldsymbol{r}_0)\rho^*(\boldsymbol{r}_0-\boldsymbol{r})\left\{\widetilde{g}(\boldsymbol{r})\ln\widetilde{g}(\boldsymbol{r})-\widetilde{h}(\boldsymbol{r})-\widetilde{h}^2(\boldsymbol{r})+e^{\widetilde{h}(\boldsymbol{r})}-\widetilde{g}(\boldsymbol{r})\right\}.&\end{aligned} \tag{72}$$

The potential difference in Equation (72) arises from the entropic cost of localizing the system in an arbitrary state. It is noted, however, that the closure given by Equations (37) and (38) applies only to Equation (72) in a metastable state characterized by $\widetilde{h}_*(\boldsymbol{r})$, which is in contrast to the Morita-Hiroike functional covering only the inter-replica TCF that necessarily satisfies the conventional closure [62,63] of the liquid-state theory due to the Legendre-transform-based formalism. That is, the generalized FP potential expressed as Equation (72) has a characteristic inherited from the original FP theory, a Landau-type theory relevant to investigate the FEL. Furthermore, Equation (72) represents that our study provides the basis of Ginzburg–Landau-type theory [79] as an extension of Landau-type one: the generalized FP potential $W(\widetilde{G})$ as a functional of local order parameter $\widetilde{h}(\boldsymbol{r})$ is a natural extension of the FP potential $V(Q)$ as a function of the global order parameter Q.

The stationary Equation (33) reveals that the new closure (37) corresponds to the mean-field equation of $W(\widetilde{G})$ given by Equation (72). The closure (37) gives the self-consistent Equation (43), similar to the previous one that predicts a dynamical transition [37,56,57]; we need to quantitatively assess the validity of Equation (43) in terms of the dynamical transitions in simulation models. Equation (10) further suggests that we can go beyond the mean-field approximation as is the case with the Ginzburg-Landau-type theory: the greatest advantage of our replica field theory is to systematically improve the self-consistent equation by considering fluctuations of inter-replica correlation field $\widetilde{h}(\boldsymbol{r})$. It remains to be addressed whether the modified self-consistent equation explains the blurring of dynamical transition into a crossover from relaxational to activated dynamics.

There is a caveat, turning our attention to the stability condition on $\widetilde{h}(\boldsymbol{r})$: translational and rotational symmetries are broken in frozen phases. The violation becomes evident by expanding $\widetilde{h}(\boldsymbol{r})$ around that at the uniform density as follows [58–60]:

$$\widetilde{h}(\boldsymbol{r}-\boldsymbol{r}';\rho^*(\boldsymbol{r})) = \widetilde{h}(\boldsymbol{r}-\boldsymbol{r}';\overline{\rho}) + \int d\boldsymbol{r}' \frac{\delta\widetilde{h}(\boldsymbol{r}-\boldsymbol{r}')}{\delta\rho}\bigg|_{\rho=\overline{\rho}} \{\rho^*(\boldsymbol{r}')-\overline{\rho}\} + \cdots . \tag{73}$$

We also have a non-perturbative approach to avoid the difficulty using a globally weighted density $\overline{\rho}_{\mathrm{WD}}$ in the inter-replica TCF: $\widetilde{h}(\boldsymbol{r}-\boldsymbol{r}';\rho^*(\boldsymbol{r})) = \widetilde{h}(\boldsymbol{r}-\boldsymbol{r}';\overline{\rho}_{\mathrm{WD}})$, according to the modified weighted density functional approximation [43,48]. Therefore, the functional derivative in Equation (36), or the new closure (37), holds approximately when either neglecting the second and higher-order terms in Equation (73) or finding $\overline{\rho}_{\mathrm{WD}}$.

The new closure (37) in a metastable state provides the self-consistent Equation (43) for the non-ergodicity parameter $f(\boldsymbol{k})$. The present field theory has demonstrated the necessity to consider higher-order contributions in the perturbative treatment for obtaining the self-consistent Equation (43) with a kernel containing the triplet DCF [76–78]: we obtain Equation (43) by adopting the approximate bridge function $B(\boldsymbol{r}) = -\widetilde{h}^2(\boldsymbol{r})/2$ beyond the RHNC approximation of $B(\boldsymbol{r}) = 0$. For comparison, we would like to mention two previous replica approaches to provide the triplet DCF in the self-consistent equation [37,56,57]. The first approach considers the perturbative contribution to the replicated HNC functional along the liquid-state theory [37]. The Legendre-transform-based method allows us to calculate the third order in $\widetilde{h}(\boldsymbol{r})$ concerning the Morita-Hiroike functional. Meanwhile, the second method considers the third-order term in density difference $\rho^*(\boldsymbol{r}) - \overline{\rho}$ by taking the Ramakrishnan-Yussouf functional of the DFT as a reference form [56,57]. Consequently, both perturbation methods amount to having the triplet DCF in the kernel of the self-consistent equation. This agreement implies the equivalence between the replicated HNC and Ramakrishnan–Yussouf approximations, consistent with the conventional results of the liquid-state theory [62].

Our scheme bears similarity to the Legendre-transform-based theory [33–38] rather than the DFT [53–57]. However, more elaborate input from the DFT [58–60] is also to be investigated, which is particularly necessary to investigate the glass transition in thin polymer films [93,94]; for example, we can improve the Ramakrishnan–Yussouf approxi-

mation by performing a variational evaluation beyond the Gaussian approximation (see Appendix B.1). Furthermore, our replica theory has two additional features arising from the field-theoretical treatment of the inter-replica TCF $\widetilde{h}(\boldsymbol{r})$ and the associated two-body interaction potential $iv_a(\boldsymbol{r})$. First, we can systematically consider fluctuations around the mean-field potential field, $v_a^*(\boldsymbol{r}) = iu(\boldsymbol{r})$, given by Equation (65), which is the same relation as that of the Legendre-transform-based method [33–38,64,86]. Second, we can develop the replica field theory to include TCF fluctuations around the metastable field $\widetilde{h}_*(\boldsymbol{r})$ as described above. Thus, the present field-theoretical formalism opens up promising avenues to advance studies on the dynamical heterogeneity in terms of the correlation function of TCF fluctuations (i.e., the so-called four-point correlation function [7–10]) as well as the FEL that includes fluctuations around a metastable state.

Funding: This research received no external funding.

Data Availability Statement: No new data were created or analyzed in this study. Data sharing is not applicable to this article.

Conflicts of Interest: The author declares no conflict of interest.

Abbreviations

Acronym	Definition
FEL	free energy landscape
DFT	density functional theory
MCT	mode coupling theory
HNC approximation	hypernetted-chain approximation
RHNC	replicated hypernetted-chain
FP potential	Franz–Parisi potential
DCF	direct correlation function
TCF	total correlation function
rhs	right-hand side
MSA	mean spherical approximation
RPA	random phase approximation

Appendix A. Proof of *Result 1*: Derivation of Equation (23) Using the Replica Trick

Equation (22) provides

$$\begin{aligned}\frac{\beta\partial\Omega_v^{(m)}}{\partial m} &= -\frac{\partial}{\partial m}\left[\ln\left\{\mathrm{Tr}_1\, e^{-\beta U_{\mathrm{intra}}(\widehat{\rho}_1)-(m-1)\beta N^* W(\widetilde{G},\widehat{\rho}_1)}\right\}\right]\\ &= \frac{\mathrm{Tr}_1\, e^{-\beta U_{\mathrm{intra}}(\widehat{\rho}_1)}\beta N^* W(\widetilde{G},\widehat{\rho}_1)\, e^{-(m-1)\beta N^* W(\widetilde{G},\widehat{\rho}_1)}}{\mathrm{Tr}_1\, e^{-\beta U_{\mathrm{intra}}(\widehat{\rho}_1)-(m-1)\beta N^* W(\widetilde{G},\widehat{\rho}_1)}}\end{aligned} \tag{A1}$$

Hence, we verify Equation (23) through the following derivation:

$$\begin{aligned}\beta N^* W(\widetilde{G}) &= \lim_{m\to 1}\frac{\beta\partial\Omega_v^{(m)}}{\partial m}\\ &= \frac{\mathrm{Tr}_1\, e^{-\beta U_{\mathrm{intra}}(\widehat{\rho}_1)}\beta N^* W(\widetilde{G},\widehat{\rho}_1)}{\mathrm{Tr}_1\, e^{-\beta U_{\mathrm{intra}}(\widehat{\rho}_1)}}\\ &= \mathrm{Tr}_1\, P_{\mathrm{eq}}(\widehat{\rho}_1)\beta N^* W(\widetilde{G},\widehat{\rho}_1)\\ &= \beta N^* W(\widetilde{G}),\end{aligned} \tag{A2}$$

where the probability $P_{\mathrm{eq}}(\widehat{\rho}_1)$ is defined by Equation (19). The last line of Equation (A2) equals the rhs of the definition (18).

Appendix B. Strong-Coupling Perturbation Theory: General Formalism

This appendix provides a general formalism of field theory for strongly-coupled glassy systems with the help of a variational approach.

Appendix B.1. Bare Interactions Mimicked by DCF: The Gibbs-Bogoliubov Inequality Approach

We first consider the grand potential $e^{-\beta\Phi_{v'}^{(m)}} = \mathbf{Tr}\, e^{-\beta U(v',\widehat{\rho})}$ for the bare interaction potential matrix v' that is adjusted to satisfy Equation (26) without the constraint $\Delta_a(\widetilde{G},\widehat{\boldsymbol{\rho}})$ by adding an inter-replica potential $\widetilde{v}(\boldsymbol{r})$ to the original potential matrix v where $\widetilde{v}(\boldsymbol{r}) = 0$. We explore an optimized interaction potential to mimic the bare interactions represented by $v'(\boldsymbol{r})$, using the Gibbs-Bogoliubov inequality for the lower bound [62,92]:

$$\beta\Phi_{v'}^{(m)} \geq \beta\Phi_{w}^{(m)} + \sum_{a=1}^{m}\sum_{b=1}^{m}\frac{1}{2}\iint d\boldsymbol{r}d\boldsymbol{r}' G_{ab}(\boldsymbol{r},\boldsymbol{r}')\{\beta v_{ab}(\boldsymbol{r}-\boldsymbol{r}') - \beta w_{ab}(\boldsymbol{r}-\boldsymbol{r}')\}. \tag{A3}$$

Maximizing the rhs of Equation (A3) with respect to $w_{ab}(\boldsymbol{r})$, we have

$$\beta w_{ab}(\boldsymbol{r}) = -c_{ab}(\boldsymbol{r}), \tag{A4}$$

in the Gaussian approximation, as shown in Appendix B.4 using the density functional integral representation of $\Phi_{w}^{(m)}$; see Equation (A35) for the equivalence between various expressions of $\Phi_{w}^{(m)}$. Accordingly, the grand potential $\Phi_{v'}^{(m)}$ can be approximated by

$$\beta\Phi_{v'}^{(m)} \approx \beta\Phi_{-k_BTc}^{(m)} + \sum_{a=1}^{m}\sum_{b=1}^{m}\frac{1}{2}\iint d\boldsymbol{r}d\boldsymbol{r}'\rho_a^*(\boldsymbol{r})\rho_b^*(\boldsymbol{r}')g_{ab}(\boldsymbol{r}-\boldsymbol{r}')\{\beta v_{ab}(\boldsymbol{r}-\boldsymbol{r}') + c_{ab}(\boldsymbol{r}-\boldsymbol{r}')\}. \tag{A5}$$

Equation (A5) reads

$$e^{-\beta\Phi_{v'}^{(m)}} = \mathbf{Tr}\, e^{-\beta U(-k_BTc,\widehat{\rho}) - \sum_{a=1}^{m}\sum_{b=1}^{m}\frac{1}{2}\iint d\boldsymbol{r}d\boldsymbol{r}'\rho_a^*(\boldsymbol{r})\rho_b^*(\boldsymbol{r}')g_{ab}(\boldsymbol{r}-\boldsymbol{r}')\{\beta v_{ab}(\boldsymbol{r}-\boldsymbol{r}')+c_{ab}(\boldsymbol{r}-\boldsymbol{r}')\}}, \tag{A6}$$

using the original definition of $e^{-\beta\Phi_{-k_BTc}^{(m)}} = \mathbf{Tr}\, e^{-\beta U(-k_BTc,\widehat{\rho})}$. For later convenience, we express $U(-k_BTc,\widehat{\boldsymbol{\rho}})$ as

$$\begin{aligned}\beta U(-k_BTc,\widehat{\boldsymbol{\rho}}) = {}& \frac{1}{8}\{c_1(\mathbf{0}) + (m-1)c(\mathbf{0})\} \\ & - \frac{1}{2}\iint d\boldsymbol{r}d\boldsymbol{r}'\{\widehat{\boldsymbol{\rho}}(\boldsymbol{r}) - \widehat{\boldsymbol{\delta}}(\boldsymbol{r})\}^{\mathrm{T}}\boldsymbol{c}(\boldsymbol{r}-\boldsymbol{r}')\left\{\widehat{\boldsymbol{\rho}}(\boldsymbol{r}') - \widehat{\boldsymbol{\delta}}(\boldsymbol{r}')\right\},\end{aligned} \tag{A7}$$

by introducing a self-energy operator,

$$\widehat{\boldsymbol{\delta}}(\boldsymbol{r}) = \frac{1}{2}\begin{pmatrix}\delta_{1a}\delta_{\mathbf{0}}\,\widehat{\rho}_1^{(1)}(\boldsymbol{r}) \\ \vdots \\ \delta_{ma}\delta_{\mathbf{0}}\,\widehat{\rho}_m^{(1)}(\boldsymbol{r})\end{pmatrix}, \tag{A8}$$

where $\delta_{na}\delta_{\mathbf{0}}$ $(1 \leq n \leq m)$ represents the operator for an intra-replica interaction potential at zero separation. The inhomogeneous Ornstein-Zernike equations given by Equations (29)–(31) are obtained from the set of maximum conditions on the variational interaction potential $w_{ab}(\boldsymbol{r})$ as follows:

$$\left.\frac{\delta\Phi_{w}^{(m)}}{\delta w_{ab}}\right|_{w_{ab}=-k_BTc_{ab}} = \frac{1}{2}\rho_a^*(\boldsymbol{r})\rho_b^*(\boldsymbol{r}')g_{ab}(\boldsymbol{r}), \tag{A9}$$

similar to the relation used in the second Legendre transform (see Appendix B.4 for details).

Appendix B.2. Evaluation Method of the Grand Potential Difference Due to the Constraint in Equation (20)

Combining Equations (20) and (A6), the grand potential difference $\Omega_{v'}^{(m)}(\widetilde{G}) - \Phi_{v'}^{(m)}$ caused by the constraint $\prod_{a=2}^{m} \Delta_a(\widetilde{G}, \widehat{\boldsymbol{\rho}})$ can be written as

$$e^{-\beta\Omega_{v'}^{(m)}(\widetilde{G})+\beta\Phi_{v'}^{(m)}} = \frac{\mathbf{Tr}\, e^{-\beta U(-k_BT\boldsymbol{c},\widehat{\boldsymbol{\rho}})} \prod_{a=2}^{m} \Delta_a(\widetilde{G}, \widehat{\boldsymbol{\rho}})}{\mathbf{Tr}\, e^{-\beta U(-k_BT\boldsymbol{c},\widehat{\boldsymbol{\rho}})}} \equiv \left\langle \prod_{a=2}^{m} \Delta_a(\widetilde{G}, \widehat{\boldsymbol{\rho}}) \right\rangle_{\boldsymbol{c}}. \tag{A10}$$

Functional-integral representation of the constraint $\prod_{a=2}^{m} \Delta_a(\widetilde{G}, \widehat{\boldsymbol{\rho}})$ in Equation (20) is

$$\begin{aligned} &\prod_{a=2}^{m} \Delta_a(\widetilde{G}, \widehat{\boldsymbol{\rho}}) \\ &= \int D'\boldsymbol{\nu} \exp\left[\sum_{a=2}^{m} \iint d\boldsymbol{r}d\boldsymbol{r}'\, i \left\{ \rho_1^*(\boldsymbol{r})\rho^*(\boldsymbol{r}')\widetilde{g}(\boldsymbol{r}-\boldsymbol{r}') - \widehat{\rho}_1^{(N)}(\boldsymbol{r})\widehat{\rho}_a^{(N)}(\boldsymbol{r}') \right\} \nu_a(\boldsymbol{r}-\boldsymbol{r}') \right], \end{aligned} \tag{A11}$$

where $\prod_{a=2}^{m} \int D\nu_a \equiv \int D'\boldsymbol{\nu}$ and $\boldsymbol{\nu} = (\nu_2, \cdots, \nu_m)^{\mathrm{T}}$. It follows from Equations (A10) and (A11) that

$$\begin{aligned} e^{-\beta\Omega_{v'}^{(m)}(\widetilde{G})+\beta\Phi_{v'}^{(m)}} = \int D'\boldsymbol{\nu}\, e^{\sum_{a=2}^{m} \iint d\boldsymbol{r}d\boldsymbol{r}'\, i\rho_1^*(\boldsymbol{r})\rho^*(\boldsymbol{r}')\widetilde{g}(\boldsymbol{r}-\boldsymbol{r}')\nu_a(\boldsymbol{r}-\boldsymbol{r}')} \\ \times \left\langle e^{-\sum_{a=2}^{m} \iint d\boldsymbol{r}d\boldsymbol{r}'\, i\widehat{\rho}_1^{(N)}(\boldsymbol{r})\widehat{\rho}_a^{(N)}(\boldsymbol{r}')\,\nu_a(\boldsymbol{r}-\boldsymbol{r}')} \right\rangle_{\boldsymbol{c}}. \end{aligned} \tag{A12}$$

We evaluate the average $\langle \mathcal{O} \rangle_{\boldsymbol{c}}$ on the rhs of Equation (A12) by developing the strong-coupling perturbation theory.

To this end, we introduce the auxiliary $\boldsymbol{\phi}$-field to have the functional-integral representation of $e^{-\beta U(-k_BT\boldsymbol{c},\widehat{\boldsymbol{\rho}})}$ as follows [79–88]:

$$\begin{aligned} e^{-\beta U(-k_BT\boldsymbol{c},\widehat{\boldsymbol{\rho}})} &= \int D\boldsymbol{\rho}\, e^{-\beta U(-k_BT\boldsymbol{c},\boldsymbol{\rho})} \prod_{b=1}^{m} \prod_{\{\boldsymbol{r}\}} \delta\left[\rho_b(\boldsymbol{r}) - \widehat{\rho}_b^{(N)}(\boldsymbol{r}) \right] \\ &= \iint D\boldsymbol{\phi}\, D\boldsymbol{\rho}\, e^{-\beta U(-k_BT\boldsymbol{c},\boldsymbol{\rho})+\int d\boldsymbol{r}\, i\boldsymbol{\phi}(\boldsymbol{r})\cdot\{\widehat{\boldsymbol{\rho}}(\boldsymbol{r})-\boldsymbol{\rho}(\boldsymbol{r})\}} \\ &= \frac{1}{\mathcal{N}_c} \int D\boldsymbol{\phi}\, e^{-\beta\mathcal{H}_0(\boldsymbol{c},\boldsymbol{\phi})+\int d\boldsymbol{r}\, i\boldsymbol{\phi}(\boldsymbol{r})\cdot\widehat{\boldsymbol{\rho}}(\boldsymbol{r})}, \end{aligned} \tag{A13}$$

where $\boldsymbol{\phi} = (\phi_1, \cdots, \phi_m)^{\mathrm{T}}$, $\prod_{a=1}^{m} \int D\phi_a \equiv \int D\boldsymbol{\phi}$, the Gaussian integration over the $\boldsymbol{\rho}$-field yields the normalization factor $\mathcal{N}_c$ written as

$$\mathcal{N}_c = \int D\boldsymbol{\phi}\, e^{\frac{1}{2}\iint d\boldsymbol{r}d\boldsymbol{r}'\boldsymbol{\phi}^{\mathrm{T}}(\boldsymbol{r})c^{-1}(\boldsymbol{r}-\boldsymbol{r}')\boldsymbol{\phi}(\boldsymbol{r}')}, \tag{A14}$$

and

$$\begin{aligned} \beta\mathcal{H}_0(\boldsymbol{c},\boldsymbol{\phi}) &= \frac{1}{8}\{c_1(\boldsymbol{0}) + (m-1)c(\boldsymbol{0})\} \\ &\quad - \frac{1}{2}\iint d\boldsymbol{r}d\boldsymbol{r}'\boldsymbol{\phi}^{\mathrm{T}}(\boldsymbol{r})\boldsymbol{c}^{-1}(\boldsymbol{r}-\boldsymbol{r}')\boldsymbol{\phi}(\boldsymbol{r}') + \int d\boldsymbol{r}\, i\boldsymbol{\phi}(\boldsymbol{r})\cdot\widehat{\boldsymbol{\delta}}(\boldsymbol{r}). \end{aligned} \tag{A15}$$

Without particles (i.e., $\widehat{\boldsymbol{\rho}} = \boldsymbol{0}$), we have

$$e^{-\beta U(-k_BT\boldsymbol{c},\widehat{\boldsymbol{\rho}}=0)} = \frac{1}{\mathcal{N}_c} \int D\boldsymbol{\phi}\, e^{-\beta\mathcal{H}_0(\boldsymbol{c},\boldsymbol{\phi})} = 1, \tag{A16}$$

consistent with the trivial result $U(-k_BT\boldsymbol{c}, \widehat{\boldsymbol{\rho}} = 0) = 0$ in Equation (A13) (see also Appendix B.5).

Meanwhile, the configurational integral represented by **Tr** provides the perturbative contribution, $\mathcal{H}_1(\boldsymbol{\nu}, \boldsymbol{\phi})$, given by

$$e^{-\beta\mathcal{H}_1(\boldsymbol{\nu},\boldsymbol{\phi})} = \mathbf{Tr}\, e^{\int d\boldsymbol{r}\, i\,\boldsymbol{\phi}(\boldsymbol{r})\cdot\widehat{\boldsymbol{\rho}}(\boldsymbol{r}) - \sum_{a=2}^{m}\iint d\boldsymbol{r}d\boldsymbol{r}'\, i\widehat{\rho}_1^{(N)}(\boldsymbol{r})\widehat{\rho}_a^{(N)}(\boldsymbol{r}')\,\nu_a(\boldsymbol{r}-\boldsymbol{r}')}. \tag{A17}$$

Defining the functional,

$$e^{-\beta\mathcal{F}(\boldsymbol{\nu})} = \frac{1}{\mathcal{N}_c}\int D\boldsymbol{\phi}\, e^{-\beta\mathcal{H}_0(\boldsymbol{c},\boldsymbol{\phi})-\beta\mathcal{H}_1(\boldsymbol{\nu},\boldsymbol{\phi})}, \tag{A18}$$

it follows from Equations (A10) and (A13) that

$$e^{-\beta\mathcal{F}(\boldsymbol{\nu}=\mathbf{0})} = e^{-\beta\Phi_{v'}^{(m)}} = \mathbf{Tr}\, e^{-\beta U(-k_BT\boldsymbol{c},\widehat{\boldsymbol{\rho}})}. \tag{A19}$$

Combining Equations (A13)–(A19), we see that the average on the rhs of Equation (A12) simply reads

$$e^{-\beta\mathcal{F}(\boldsymbol{\nu})+\beta\mathcal{F}(\boldsymbol{\nu}=\mathbf{0})} = \left\langle e^{-\sum_{a=2}^{m}\iint d\boldsymbol{r}d\boldsymbol{r}'\, i\widehat{\rho}_1^{(N)}(\boldsymbol{r})\widehat{\rho}_a^{(N)}(\boldsymbol{r}')\,\nu_a(\boldsymbol{r}-\boldsymbol{r}')}\right\rangle_{\boldsymbol{c}}. \tag{A20}$$

Equations (A17)–(A20) indicate that the remaining task is to properly evaluate the perturbative contribution $\mathcal{H}_1(\boldsymbol{\nu}, \boldsymbol{\phi})$ in Equation (A18) at strong coupling.

Appendix B.3. Strong-Coupling Expansion

Equation (24) implies that

$$e^{\beta\mu-\frac{c_{aa}(\mathbf{0})}{2}} = \frac{N^*}{\int d\boldsymbol{r}e^{\sum_{b=1}^{m}\int d\boldsymbol{r}'c_{ab}(\boldsymbol{r}-\boldsymbol{r}')\rho_b^*(\boldsymbol{r}')}} \approx \overline{\rho}, \tag{A21}$$

considering the finite range of the DCF. It follows from Equation (A21) that the fugacity $e^{\beta\mu}$ becomes

$$e^{\beta\mu} \approx \frac{\overline{\rho}}{\gamma_a} \tag{A22}$$

by introducing the coupling parameter γ_a defined as follows:

$$\gamma_a = e^{-\frac{c_{aa}(\mathbf{0})}{2}}, \tag{A23}$$

or $\gamma_1 = e^{-\frac{c_1(\mathbf{0})}{2}}$ for $a = 1$ and $\gamma = e^{-\frac{c(\mathbf{0})}{2}}$ for $a \geq 2$.

The relation (A22) clarifies that the fugacity expansion method is validated at strong coupling, or in the glassy state. In what follows, we set $\gamma = \gamma_a$ for brevity considering that the glassy state is located in the strong-coupling regime of γ_1, $\gamma \gg 1$ because of $-c_1(\mathbf{0})$, $-c(\mathbf{0}) \gg 1$ at freezing [95]. The strong-coupling perturbation theory is based on the use of the following expansion:

$$\mathbf{Tr} = 1 + \frac{\overline{\rho}}{\gamma}\sum_{a=1}^{m}\int d\boldsymbol{r}_{a,1} + \left(\frac{\overline{\rho}}{\gamma}\right)^2\left(\frac{1}{2}\sum_{a=1}^{m}\iint d\boldsymbol{r}_{a,1}d\boldsymbol{r}_{a,2} + \sum_{a(>b)}\sum_{b=1}^{m}\iint d\boldsymbol{r}_{a,1}d\boldsymbol{r}_{b,1}\right) + \mathcal{O}\left[\gamma^{-3}\right]. \tag{A24}$$

Substituting Equation (A24) into Equation (A17), we obtain

$$\begin{aligned} -\beta\mathcal{H}_1(\boldsymbol{\nu},\boldsymbol{\phi}) &= \ln\left\{\mathbf{Tr}\, e^{\int d\boldsymbol{r}\, i\boldsymbol{\phi}(\boldsymbol{r})\cdot\widehat{\boldsymbol{\rho}}(\boldsymbol{r})-\sum_{a=2}^{m}\iint d\boldsymbol{r}d\boldsymbol{r}'\, i\widehat{\rho}_a^{(N)}(\boldsymbol{r})\widehat{\rho}_1^{(N)}(\boldsymbol{r}')\,\nu_a(\boldsymbol{r}-\boldsymbol{r}')}\right\} \\ &\approx \ln\left\{1+\frac{\overline{\rho}}{\gamma}\mathcal{U}_1(\boldsymbol{\phi})+\left(\frac{\overline{\rho}}{\gamma}\right)^2\mathcal{U}_2(\boldsymbol{\phi})\right\} \\ &\approx \frac{\overline{\rho}}{\gamma}\mathcal{U}_1(\boldsymbol{\phi})+\left(\frac{\overline{\rho}}{\gamma}\right)^2\left\{\mathcal{U}_2(\boldsymbol{\phi})-\frac{1}{2}\mathcal{U}_1^2(\boldsymbol{\phi})\right\}, \end{aligned} \tag{A25}$$

where

$$\mathcal{U}_1(\boldsymbol{\phi}) = \sum_{a=1}^{m}\int d\boldsymbol{r}_{a,1}\, e^{\int d\boldsymbol{r} i\phi_a(\boldsymbol{r})\widehat{\rho}_a^{(1)}(\boldsymbol{r})}, \tag{A26}$$

$$\begin{aligned} \mathcal{U}_2(\boldsymbol{\phi}) &= \frac{1}{2}\sum_{a=1}^{m}\iint d\boldsymbol{r}_{a,1}d\boldsymbol{r}_{a,2}\, e^{\int d\boldsymbol{r} i\phi_a(\boldsymbol{r})\widehat{\rho}_a^{(2)}(\boldsymbol{r})} \\ &\quad+\sum_{a(>b)}\sum_{b=2}^{m}\iint d\boldsymbol{r}_{a,1}d\boldsymbol{r}_{b,1}\, e^{\int d\boldsymbol{r}\, i\phi_a(\boldsymbol{r})\left\{\widehat{\rho}_a^{(1)}(\boldsymbol{r})+\widehat{\rho}_b^{(1)}(\boldsymbol{r})\right\}} \\ &\quad+\sum_{a=2}^{m}\iint d\boldsymbol{r}_{a,1}d\boldsymbol{r}_{1,1}\, e^{\int d\boldsymbol{r}\left\{i\phi_1(\boldsymbol{r})\widehat{\rho}_1^{(1)}(\boldsymbol{r})+i\phi_a(\boldsymbol{r})\widehat{\rho}_a^{(1)}(\boldsymbol{r})\right\}-\iint d\boldsymbol{r}d\boldsymbol{r}'\, i\widehat{\rho}_1^{(1)}(\boldsymbol{r})\widehat{\rho}_a^{(1)}(\boldsymbol{r}')\nu_a(\boldsymbol{r}-\boldsymbol{r}')}. \end{aligned} \tag{A27}$$

Rearranging the terms in Equations (A26) and (A27), we have

$$\mathcal{U}_2(\boldsymbol{\phi})-\frac{1}{2}\mathcal{U}_1^2(\boldsymbol{\phi}) = \sum_{a=2}^{m}\iint d\boldsymbol{r}_{1,1}d\boldsymbol{r}_{a,1}\, e^{\int d\boldsymbol{r}\left\{i\phi_1(\boldsymbol{r})\widehat{\rho}_1^{(1)}(\boldsymbol{r})+i\phi_a(\boldsymbol{r})\widehat{\rho}_a^{(1)}(\boldsymbol{r})\right\}} f(i\nu_a), \tag{A28}$$

using the Mayer f-function:

$$f(i\nu_a) = e^{-i\nu_a(\boldsymbol{r}_{1,1}-\boldsymbol{r}_{a,1})}-1. \tag{A29}$$

It is found from Equations (A25) and (A28) that Equation (A18) is approximated by

$$e^{-\beta\mathcal{F}(\nu)} = \frac{1}{\mathcal{N}_c}\int D\boldsymbol{\phi}\, e^{-\beta\mathcal{H}_{\mathrm{mf}}(\boldsymbol{\phi})}\left\{1+\left(\frac{\overline{\rho}}{\gamma}\right)^2\sum_{a=2}^{m}\iint d\boldsymbol{r}d\boldsymbol{r}'\, e^{i\phi_1(\boldsymbol{r})+i\phi_a(\boldsymbol{r}')}f(i\nu_a)\right\}, \tag{A30}$$

where

$$\beta\mathcal{H}_{\mathrm{mf}}(\boldsymbol{\phi}) = \beta\mathcal{H}_0(\boldsymbol{c},\boldsymbol{\phi})-\frac{\overline{\rho}}{\gamma}\mathcal{U}_1(\boldsymbol{\phi}). \tag{A31}$$

Equations (A19), (A29) and (A30) imply that

$$e^{-\beta\Phi^{(m)}_{-k_BTc}} = e^{-\beta\mathcal{F}(\boldsymbol{\nu}=\mathbf{0})} = \frac{1}{\mathcal{N}_c}\int D\boldsymbol{\phi}\, e^{-\beta\mathcal{H}_{\mathrm{mf}}(\boldsymbol{\phi})} \tag{A32}$$

because of $f(i\nu_a=0)=0$. Combining Equations (A30) and (A32), we obtain the following approximate result at strong coupling:

$$\beta\mathcal{F}(\boldsymbol{\nu})-\beta\mathcal{F}(\boldsymbol{\nu}=\mathbf{0}) = -\left(\frac{\overline{\rho}}{\gamma}\right)^2\sum_{a=2}^{m}\iint d\boldsymbol{r}_{1,1}d\boldsymbol{r}_{a,1}\left\langle e^{\int d\boldsymbol{r}\left\{i\phi_1(\boldsymbol{r})\widehat{\rho}_1^{(1)}(\boldsymbol{r})+i\phi_a(\boldsymbol{r})\widehat{\rho}_a^{(1)}(\boldsymbol{r})\right\}}\right\rangle_{\phi} f(i\nu_a), \tag{A33}$$

where the subscript ϕ denotes the averaging procedure as follows:

$$\langle \mathcal{O} \rangle_{\phi} = \frac{\int D\boldsymbol{\phi}\, \mathcal{O}\, e^{-\beta \mathcal{H}_{\mathrm{mf}}(\boldsymbol{\phi})}}{\int D\boldsymbol{\phi}\, e^{-\beta \mathcal{H}_{\mathrm{mf}}(\boldsymbol{\phi})}}. \tag{A34}$$

Equation (A33) is a representative result of the strong-coupling perturbation theory developed in this section.

Appendix B.4. Verifying Equation (A4) in the Gaussian Approximation

To evaluate density-density correlations, it is straightforward to use the density functional integral representation of $\Phi_{w}^{(m)}(\widetilde{G})$ expressed as [84–88]

$$\begin{aligned} e^{-\beta \Phi_{w}^{(m)}(\widetilde{G})} &= \mathbf{Tr}\, e^{-\beta U(\boldsymbol{w}, \widehat{\boldsymbol{\rho}})} \\ &= \int D\boldsymbol{\rho}\, \mathbf{Tr}\, e^{-\beta U(\boldsymbol{w}, \boldsymbol{\rho})} \prod_{b=1}^{m} \prod_{\{\boldsymbol{r}\}} \delta\left[\rho_b(\boldsymbol{r}) - \widehat{\rho}_b^{(N)}(\boldsymbol{r})\right] \\ &= \int D\boldsymbol{\rho}\, e^{-\beta F_{\mathrm{mf}}(\boldsymbol{w}, \boldsymbol{\rho})}, \end{aligned} \tag{A35}$$

using the density functional $F_{\mathrm{mf}}(\boldsymbol{w}, \boldsymbol{\rho})$ defined by Equation (49). Equation (A35) leads to

$$\frac{\delta \Phi_{w}^{(m)}}{\delta w_{ab}} = \frac{1}{2} \left\langle \rho_a(\boldsymbol{r}) \rho_b(\boldsymbol{r}') \right\rangle_{\rho} \tag{A36}$$

for the left-hand side of Equation (A9). The subscript ρ in Equation (A36) represents the following average:

$$\langle \mathcal{O} \rangle_{\rho} = \frac{\int D\boldsymbol{\rho}\, \mathcal{O}\, e^{-\beta F_{\mathrm{mf}}(\boldsymbol{w}, \boldsymbol{\rho})}}{e^{-\beta \Phi_{w}^{(m)}(\widetilde{G})}}. \tag{A37}$$

It is also noted that the saddle-point equation $\delta F_{\mathrm{mf}} / \delta \rho_a|_{\rho = \rho_a^*} = 0$ in Equation (A35) provides

$$\rho_a^*(\boldsymbol{r}) = e^{\beta \mu + \frac{\beta w_{aa}(\mathbf{0})}{2}} \exp\left\{ - \sum_{b=1}^{m} \int d\boldsymbol{r}' \beta w_{ab}(\boldsymbol{r} - \boldsymbol{r}') \rho_b^*(\boldsymbol{r}') \right\}, \tag{A38}$$

which matches Equation (24) when Equation (A4) is verified.

Let $\boldsymbol{n} = \boldsymbol{\rho} - \boldsymbol{\rho}^*$ be a fluctuating density vector. In the saddle-point approximation, the mean density-density correlation appearing in the rhs of Equation (A36) reads

$$\left\langle \rho_a(\boldsymbol{r}) \rho_b(\boldsymbol{r}') \right\rangle_{\rho} = \rho_a^*(\boldsymbol{r}) \rho_b^*(\boldsymbol{r}') + \left\langle n_a(\boldsymbol{r}) n_b(\boldsymbol{r}') \right\rangle_{\rho}. \tag{A39}$$

The correlation function $N_{ab}(\boldsymbol{r} - \boldsymbol{r}') = \langle n_a(\boldsymbol{r}) n_b(\boldsymbol{r}') \rangle_{\rho}$ in Equation (A39) corresponds to the matrix element of density-density correlation matrix $\boldsymbol{N} = \left\langle \boldsymbol{n}\boldsymbol{n}^{\mathrm{T}} \right\rangle_{\rho}$. If the equality (A9) holds, Equations (A36) and (A39) imply that $N_{ab}(\boldsymbol{r} - \boldsymbol{r}')$ is related to the TCF $h_{ab}(\boldsymbol{r}) = g_{ab}(\boldsymbol{r}) - 1$ as

$$N_{ab}(\boldsymbol{r} - \boldsymbol{r}') = \rho_a^*(\boldsymbol{r}) \delta_{ab} \delta(\boldsymbol{r} - \boldsymbol{r}') + \rho_a^*(\boldsymbol{r}) \rho_b^*(\boldsymbol{r}') h_{ab}(\boldsymbol{r} - \boldsymbol{r}'). \tag{A40}$$

Meanwhile, the matrix element $N_{ab}^{-1}(\boldsymbol{r} - \boldsymbol{r}')$ of the inverse matrix $\boldsymbol{N}^{-1}$ is given by

$$N_{ab}^{-1}(\boldsymbol{r} - \boldsymbol{r}') = \beta w_{ab}(\boldsymbol{r} - \boldsymbol{r}') + \frac{\delta_{ab} \delta(\boldsymbol{r} - \boldsymbol{r}')}{\rho_a^*(\boldsymbol{r})}, \tag{A41}$$

when considering Gaussian fluctuations of $\boldsymbol{n}(\boldsymbol{r})$.

The inverse matrix $\boldsymbol{N}^{-1}(\boldsymbol{r}-\boldsymbol{r}'')$ satisfies $\int d\boldsymbol{r}''\boldsymbol{N}^{-1}(\boldsymbol{r}-\boldsymbol{r}'')\boldsymbol{N}(\boldsymbol{r}''-\boldsymbol{r}') = \delta(\boldsymbol{r}-\boldsymbol{r}')\boldsymbol{I}$, or

$$\sum_{b=1}^{m}\int d\boldsymbol{r}''N_{ab}^{-1}(\boldsymbol{r}-\boldsymbol{r}'')N_{bc}(\boldsymbol{r}''-\boldsymbol{r}') = \delta_{ac}\delta(\boldsymbol{r}-\boldsymbol{r}'). \tag{A42}$$

Substituting Equations (A40) and (A41) into Equation (A42), the left-hand side of Equation (A42) is reduced to

$$\begin{aligned}
&\sum_{b=1}^{m}\int d\boldsymbol{r}''\left\{\beta w_{ab}(\boldsymbol{r}-\boldsymbol{r}'')+\frac{\delta_{ab}\delta(\boldsymbol{r}-\boldsymbol{r}'')}{\rho_a^*(\boldsymbol{r})}\right\}\rho_b^*(\boldsymbol{r}'')\delta_{bc}\delta(\boldsymbol{r}''-\boldsymbol{r}')\\
&\quad+\sum_{b=1}^{m}\int d\boldsymbol{r}''\left\{\beta w_{ab}(\boldsymbol{r}-\boldsymbol{r}'')+\frac{\delta_{ab}\delta(\boldsymbol{r}-\boldsymbol{r}'')}{\rho_a^*(\boldsymbol{r})}\right\}\rho_b^*(\boldsymbol{r}'')\rho_c^*(\boldsymbol{r}')h_{bc}(\boldsymbol{r}''-\boldsymbol{r}')\\
&\quad=\rho_c^*(\boldsymbol{r}')\beta w_{ac}(\boldsymbol{r}-\boldsymbol{r}')+\delta_{ac}\delta(\boldsymbol{r}-\boldsymbol{r}')\\
&\quad\quad+\sum_{b=1}^{m}\int d\boldsymbol{r}''\rho_b^*(\boldsymbol{r}'')\rho_c^*(\boldsymbol{r}')\beta w_{ab}(\boldsymbol{r}-\boldsymbol{r}'')h_{bc}(\boldsymbol{r}''-\boldsymbol{r}')+\rho_c^*(\boldsymbol{r}')h_{ac}(\boldsymbol{r}-\boldsymbol{r}').
\end{aligned}\tag{A43}$$

It follows from Equations (A42) and (A43) that

$$h_{ac}(\boldsymbol{r}-\boldsymbol{r}') = -\beta w_{ac}(\boldsymbol{r}-\boldsymbol{r}')-\sum_{b=1}^{m}\int d\boldsymbol{r}''\rho_b^*(\boldsymbol{r}'')\beta w_{ab}(\boldsymbol{r}-\boldsymbol{r}'')h_{bc}(\boldsymbol{r}''-\boldsymbol{r}'), \tag{A44}$$

which becomes the inhomogeneous Ornstein-Zernike Equation (29) when Equation (A4) holds. Namely, combination of the maximum condition (A9) with the inhomogeneous Ornstein-Zernike Equation (29) verifies Equation (A4).

Appendix B.5. Derivation of Equation (A16)

Let us rearrange $\mathcal{H}_0(\boldsymbol{c},\boldsymbol{\phi})$ in Equation (A15) by completing the square. To this end, we define an imaginary potential vector,

$$\boldsymbol{\zeta}_c(\boldsymbol{r}) = i\int d\boldsymbol{r}'\boldsymbol{c}(\boldsymbol{r}-\boldsymbol{r}')\widehat{\boldsymbol{\delta}}(\boldsymbol{r}'), \tag{A45}$$

with which Equation (A15) is transformed into

$$\beta\mathcal{H}_0(\boldsymbol{c},\boldsymbol{\phi}) = -\frac{1}{2}\iint d\boldsymbol{r}d\boldsymbol{r}'\left\{\boldsymbol{\phi}^{\mathrm{T}}(\boldsymbol{r})-\boldsymbol{\zeta}_c^{\mathrm{T}}(\boldsymbol{r})\right\}\boldsymbol{c}^{-1}(\boldsymbol{r}-\boldsymbol{r}')\{\boldsymbol{\phi}(\boldsymbol{r}')-\boldsymbol{\zeta}_c(\boldsymbol{r}')\}, \tag{A46}$$

noting that

$$-\frac{1}{2}\iint d\boldsymbol{r}d\boldsymbol{r}'\boldsymbol{\zeta}_c^{\mathrm{T}}(\boldsymbol{r})\boldsymbol{c}^{-1}(\boldsymbol{r}-\boldsymbol{r}')\boldsymbol{\zeta}_c(\boldsymbol{r}') = \frac{1}{8}\{c_1(\boldsymbol{0})+(m-1)c(\boldsymbol{0})\}. \tag{A47}$$

It is found from Equation (A46) that

$$\int D\boldsymbol{\phi}\, e^{-\beta\mathcal{H}_0(\boldsymbol{c},\boldsymbol{\phi})} = \mathcal{N}_c, \tag{A48}$$

which is equivalent to Equation (A16).

Appendix C. Derivation of Equation (51)

The key functional $\mathcal{H}_{\rm mf}(\boldsymbol{\phi})$ in the $\boldsymbol{\phi}$–functional integral of Equation (A30) consists of two terms as seen from Equation (A31). The first contribution $\beta\mathcal{H}_0(\boldsymbol{c},\boldsymbol{\phi})$ to $\mathcal{H}_{\rm mf}(\boldsymbol{\phi})$ at the saddle-point path $\boldsymbol{\phi}=i\boldsymbol{\psi}^*$ is written as

$$\begin{aligned}
&\beta\mathcal{H}_0(\boldsymbol{c},i\boldsymbol{\psi}^*)-\frac{1}{8}\{c_1(\mathbf{0})+(m-1)c(\mathbf{0})\}\\
&\quad=\frac{1}{2}\iint d\boldsymbol{r}d\boldsymbol{r}'\boldsymbol{\psi}^*(\boldsymbol{r})^{\rm T}\boldsymbol{c}^{-1}(\boldsymbol{r}-\boldsymbol{r}')\boldsymbol{\psi}^*(\boldsymbol{r}')-\int d\boldsymbol{r}\,\boldsymbol{\psi}^*(\boldsymbol{r})\cdot\widehat{\boldsymbol{\delta}}(\boldsymbol{r})\\
&\quad=\frac{1}{2}\iint d\boldsymbol{r}d\boldsymbol{r}'\boldsymbol{\rho}^*(\boldsymbol{r})^{\rm T}\boldsymbol{c}(\boldsymbol{r}-\boldsymbol{r}')\boldsymbol{\rho}^*(\boldsymbol{r}')-\int d\boldsymbol{r}\,\boldsymbol{\psi}^*(\boldsymbol{r})\cdot\widehat{\boldsymbol{\delta}}(\boldsymbol{r})\\
&\qquad\qquad-\sum_{a=1}^{m}\int d\boldsymbol{r}\,\frac{\rho_a^*(\boldsymbol{r})}{2}c(\mathbf{0})+\frac{1}{8}\{c_1(\mathbf{0})+(m-1)c(\mathbf{0})\}\\
&\quad=\frac{1}{2}\iint d\boldsymbol{r}d\boldsymbol{r}'\boldsymbol{\rho}^*(\boldsymbol{r})^{\rm T}\boldsymbol{c}(\boldsymbol{r}-\boldsymbol{r}')\boldsymbol{\rho}^*(\boldsymbol{r}')-\frac{1}{4}\{c_1(\mathbf{0})+(m-1)c(\mathbf{0})\}+\sum_{a=1}^{m}\int d\boldsymbol{r}\,\frac{\rho_a^*(\boldsymbol{r})}{2}c(\mathbf{0})\\
&\qquad\qquad-\sum_{a=1}^{m}\int d\boldsymbol{r}\,\frac{\rho_a^*(\boldsymbol{r})}{2}c(\mathbf{0})+\frac{1}{8}\{c_1(\mathbf{0})+(m-1)c(\mathbf{0})\}\\
&\quad=\frac{1}{2}\iint d\boldsymbol{r}d\boldsymbol{r}'\boldsymbol{\rho}^*(\boldsymbol{r})^{\rm T}\boldsymbol{c}(\boldsymbol{r}-\boldsymbol{r}')\boldsymbol{\rho}^*(\boldsymbol{r}')-\frac{1}{8}\{c_1(\mathbf{0})+(m-1)c(\mathbf{0})\},
\end{aligned}\tag{A49}$$

where use has been made of the relation, $\rho_a^*(\boldsymbol{r})=e^{\beta\mu-\psi_a^*(\boldsymbol{r})}$. Hence, Equation (A31) leads to

$$\begin{aligned}
\mathcal{H}_{\rm mf}(i\boldsymbol{\psi}^*)&=\beta\mathcal{H}_0(\boldsymbol{c},i\boldsymbol{\psi}^*)-\frac{\overline{\rho}}{\gamma}\mathcal{U}_1(i\boldsymbol{\psi}^*)\\
&=\frac{1}{2}\iint d\boldsymbol{r}d\boldsymbol{r}'\boldsymbol{\rho}^*(\boldsymbol{r})^{\rm T}\boldsymbol{c}(\boldsymbol{r}-\boldsymbol{r}')\boldsymbol{\rho}^*(\boldsymbol{r}')-\sum_{a=1}^{m}\int d\boldsymbol{r}\,\rho_a^*(\boldsymbol{r})\\
&=\beta F_{\rm mf}(-k_BT\boldsymbol{c},\boldsymbol{\rho}^*).
\end{aligned}\tag{A50}$$

Thus, we verify the equality in Equation (51) from Equations (A49) and (A50) in detail.

Appendix D. Derivation of Equation (53)

We can demonstrate that the inhomogeneous Ornstein-Zernike Equation (29) is equivalent to Equation (53). First, Equation (29) becomes

$$\begin{aligned}
&\sum_{b=1}^{m}\int d\boldsymbol{r}''\,c_{ab}^{-1}(\boldsymbol{r}-\boldsymbol{r}'')h_{bc}(\boldsymbol{r}''-\boldsymbol{r}')\\
&=\sum_{b=1}^{m}\int d\boldsymbol{r}''\left\{c_{ab}^{-1}(\boldsymbol{r}-\boldsymbol{r}'')c_{bc}(\boldsymbol{r}''-\boldsymbol{r}')+\sum_{d=1}^{m}\int d\boldsymbol{u}\,\rho_d^*(\boldsymbol{u})c_{ab}^{-1}(\boldsymbol{r}-\boldsymbol{r}'')c_{bd}(\boldsymbol{r}''-\boldsymbol{u}))h_{dc}(\boldsymbol{u}-\boldsymbol{r}')\right\}\\
&=\delta_{ac}\delta(\boldsymbol{r}-\boldsymbol{r}')+\sum_{d=1}^{m}\int d\boldsymbol{u}\,\rho_d^*(\boldsymbol{u})\delta_{ad}\delta(\boldsymbol{r}-\boldsymbol{u}))h_{dc}(\boldsymbol{u}-\boldsymbol{r}')\\
&=\delta_{ac}\delta(\boldsymbol{r}-\boldsymbol{r}')+\rho_a^*(\boldsymbol{r})h_{ac}(\boldsymbol{r}-\boldsymbol{r}').
\end{aligned}\tag{A51}$$

Furthermore, both the left-hand side and the rhs in the last line of Equation (A51) are transformed into

$$\begin{aligned}
&\sum_{b=1}^{m}\sum_{c=1}^{m}\iint d\boldsymbol{r}''d\boldsymbol{r}'\,c_{ab}^{-1}(\boldsymbol{r}-\boldsymbol{r}'')h_{bc}(\boldsymbol{r}''-\boldsymbol{r}')h_{cd}^{-1}(\boldsymbol{r}'-\boldsymbol{u})\\
&\qquad=\sum_{b=1}^{m}\int d\boldsymbol{r}''\,c_{ab}^{-1}(\boldsymbol{r}-\boldsymbol{r}'')\delta_{bd}\delta(\boldsymbol{r}''-\boldsymbol{u})\\
&\qquad=c_{ad}^{-1}(\boldsymbol{r}-\boldsymbol{u})
\end{aligned}\tag{A52}$$

and

$$\sum_{c=1}^{m}\int d\boldsymbol{r}'\left\{\delta_{ac}\delta(\boldsymbol{r}-\boldsymbol{r}')h_{cd}^{-1}(\boldsymbol{r}'-\boldsymbol{u})+\rho_a^*(\boldsymbol{r})h_{ac}(\boldsymbol{r}-\boldsymbol{r}')h_{cd}^{-1}(\boldsymbol{r}'-\boldsymbol{u})\right\}$$
$$=h_{ad}^{-1}(\boldsymbol{r}-\boldsymbol{u})+\rho_a^*(\boldsymbol{r})\delta_{ad}\delta(\boldsymbol{r}-\boldsymbol{u}), \tag{A53}$$

respectively. Thus, we have proved that the inhomogeneous Ornstein-Zernike Equation (29) reads Equation (53).

Appendix E. Derivation of Equation (60)

We consider m replicas that have two particles in total: there is one particle, respectively, in replica 1 and replica a, and no particle exists in the other replicas. Let $\widehat{\boldsymbol{\rho}}_{(1)}(\boldsymbol{r})\equiv(\rho_{1,1}^{(1)}(\boldsymbol{r}),0,\cdots,0,\rho_{a,1}^{(1)}(\boldsymbol{r}),0,\cdots)$ be the one-particle density vector in this system. We need to rearrange the sum of $\beta\mathcal{H}_0(\boldsymbol{h},\boldsymbol{\varphi})$ and a one-particle energy $-i\int d\boldsymbol{r}\boldsymbol{\varphi}(\boldsymbol{r})\cdot\widehat{\boldsymbol{\rho}}_{(1)}(\boldsymbol{r})$ for the φ–averaging in Equation (60). For later convenience, we introduce a fluctuating potential that shifts to

$$\boldsymbol{\varphi}_\zeta(\boldsymbol{r})=\boldsymbol{\varphi}(\boldsymbol{r})+\boldsymbol{\zeta}_1(\boldsymbol{r})-\boldsymbol{\zeta}_h(\boldsymbol{r}) \tag{A54}$$

using a reference potential,

$$\boldsymbol{\zeta}_1(\boldsymbol{r})=i\int d\boldsymbol{r}'\boldsymbol{h}(\boldsymbol{r}-\boldsymbol{r}')\widehat{\boldsymbol{\rho}}_{(1)}(\boldsymbol{r}'), \tag{A55}$$

in addition to

$$\boldsymbol{\zeta}_h(\boldsymbol{r})=i\int d\boldsymbol{r}'\boldsymbol{h}(\boldsymbol{r}-\boldsymbol{r}')\widehat{\delta}(\boldsymbol{r}'), \tag{A56}$$

similar to Equation (A45).

We note that

$$-\iint d\boldsymbol{r}d\boldsymbol{r}'\boldsymbol{\zeta}_h^{\mathrm{T}}(\boldsymbol{r})\boldsymbol{h}^{-1}(\boldsymbol{r}-\boldsymbol{r}')\boldsymbol{\zeta}_1(\boldsymbol{r}')=\frac{1}{2}\int d\boldsymbol{r}\widehat{\boldsymbol{\rho}}_{(1)}^{\mathrm{T}}(\boldsymbol{r})\boldsymbol{h}(\boldsymbol{r}-\boldsymbol{r}')\delta(\boldsymbol{r}-\boldsymbol{r}') \tag{A57}$$

and that

$$-\frac{1}{2}\iint d\boldsymbol{r}d\boldsymbol{r}'\boldsymbol{\zeta}_h^{\mathrm{T}}(\boldsymbol{r})\boldsymbol{h}^{-1}(\boldsymbol{r}-\boldsymbol{r}')\boldsymbol{\zeta}_h(\boldsymbol{r}')=\frac{1}{8}\{h_1(\boldsymbol{0})+(m-1)h(\boldsymbol{0})\}, \tag{A58}$$

similar to Equation (A47). Completing the square, we have

$$\beta\mathcal{H}_0(\boldsymbol{h},\boldsymbol{\varphi})-i\int d\boldsymbol{r}\boldsymbol{\varphi}(\boldsymbol{r})\cdot\widehat{\boldsymbol{\rho}}^{(1)}(\boldsymbol{r})=-\frac{1}{2}\iint d\boldsymbol{r}d\boldsymbol{r}'\boldsymbol{\varphi}_\zeta^{\mathrm{T}}(\boldsymbol{r})\boldsymbol{h}^{-1}(\boldsymbol{r}-\boldsymbol{r}')\boldsymbol{\varphi}_\zeta(\boldsymbol{r}')+\beta\mathcal{H}_\zeta, \tag{A59}$$

where

$$\begin{aligned}\beta\mathcal{H}_\zeta=&\frac{1}{2}\iint d\boldsymbol{r}d\boldsymbol{r}'\{\boldsymbol{\zeta}_1(\boldsymbol{r})-\boldsymbol{\zeta}_h(\boldsymbol{r})\}^{\mathrm{T}}\boldsymbol{h}^{-1}(\boldsymbol{r}-\boldsymbol{r}')\{\boldsymbol{\zeta}_1(\boldsymbol{r}')-\boldsymbol{\zeta}_h(\boldsymbol{r}')\}\\&-\frac{1}{2}\iint d\boldsymbol{r}d\boldsymbol{r}'\boldsymbol{\zeta}_h^{\mathrm{T}}(\boldsymbol{r})\boldsymbol{h}^{-1}(\boldsymbol{r}-\boldsymbol{r}')\boldsymbol{\zeta}_h(\boldsymbol{r}')\\=&-\frac{1}{2}\iint d\boldsymbol{r}d\boldsymbol{r}'\left\{\widehat{\boldsymbol{\rho}}_{(1)}^{\mathrm{T}}(\boldsymbol{r})\boldsymbol{h}(\boldsymbol{r}-\boldsymbol{r}')\widehat{\boldsymbol{\rho}}_{(1)}(\boldsymbol{r}')-\widehat{\boldsymbol{\rho}}_{(1)}^{\mathrm{T}}(\boldsymbol{r})\boldsymbol{h}(\boldsymbol{r}-\boldsymbol{r}')\delta(\boldsymbol{r}-\boldsymbol{r}')\right\}\\=&-\iint d\boldsymbol{r}d\boldsymbol{r}'\widehat{\rho}_{1,1}^{(1)}(\boldsymbol{r})\widehat{\rho}_{a,1}^{(1)}(\boldsymbol{r})\widetilde{h}(\boldsymbol{r}-\boldsymbol{r}')=-\widetilde{h}(\boldsymbol{r}_{1,1}-\boldsymbol{r}_{a,1}),\end{aligned} \tag{A60}$$

thus verifying the result in Equation (60).

Appendix F. Verifying the First Term on the rhs of Equation (36)

The Ornstein-Zernike Equation (31) at $m = 1$ yields approximately

$$\begin{aligned}\widetilde{c}(\boldsymbol{r}_0 - \boldsymbol{r}') =& \widetilde{h}(\boldsymbol{r}_0 - \boldsymbol{r}') \\ &- \int d\boldsymbol{r}'' \Big\{ \rho^*(\boldsymbol{r}'') \widetilde{h}(\boldsymbol{r}_0 - \boldsymbol{r}'') h(\boldsymbol{r}'' - \boldsymbol{r}') + \rho^*(\boldsymbol{r}'') c(\boldsymbol{r}_0 - \boldsymbol{r}'') \widetilde{h}(\boldsymbol{r}'' - \boldsymbol{r}') \Big\} + \mathcal{O}[\widetilde{h}^2]. \end{aligned} \tag{A61}$$

Substituting Equation (A61) into Equation (35), the logarithmic contribution $\mathcal{L}(\widetilde{h})$ in Equation (34) becomes

$$\begin{aligned}\mathcal{L}(\widetilde{h}) =& \frac{1}{2} \iint d\boldsymbol{r}_0 d\boldsymbol{r}' \, \rho^*(\boldsymbol{r}_0) \rho^*(\boldsymbol{r}') \widetilde{c}(\boldsymbol{r}_0 - \boldsymbol{r}') \widetilde{h}(\boldsymbol{r}_0 - \boldsymbol{r}') \\ =& \frac{1}{2} \iint d\boldsymbol{r}_0 d\boldsymbol{r}' \, \rho^*(\boldsymbol{r}_0) \rho^*(\boldsymbol{r}') \widetilde{h}^2(\boldsymbol{r}_0 - \boldsymbol{r}') \\ &- \frac{1}{2} \iiint d\boldsymbol{r}_0 d\boldsymbol{r}' d\boldsymbol{r}'' \, \rho^*(\boldsymbol{r}_0) \rho^*(\boldsymbol{r}') \rho^*(\boldsymbol{r}'') \widetilde{h}(\boldsymbol{r}_0 - \boldsymbol{r}'') h(\boldsymbol{r}'' - \boldsymbol{r}') \widetilde{h}(\boldsymbol{r}_0 - \boldsymbol{r}') \\ &- \frac{1}{2} \iiint d\boldsymbol{r}_0 d\boldsymbol{r}' d\boldsymbol{r}'' \, \rho^*(\boldsymbol{r}_0) \rho^*(\boldsymbol{r}') \rho^*(\boldsymbol{r}'') c(\boldsymbol{r}_0 - \boldsymbol{r}'') \widetilde{h}(\boldsymbol{r}'' - \boldsymbol{r}') \widetilde{h}(\boldsymbol{r}_0 - \boldsymbol{r}') + \mathcal{O}[\widetilde{h}^3]. \end{aligned} \tag{A62}$$

The derivative with respect to $\widetilde{h}(\boldsymbol{r})$ gives

$$\begin{aligned}&\frac{\delta \mathcal{L}(\widetilde{h})}{\delta \widetilde{h}(\boldsymbol{r})} \\ &\approx \iint d\boldsymbol{r}_0 d\boldsymbol{r}' \, \rho^*(\boldsymbol{r}_0) \rho^*(\boldsymbol{r}') \widetilde{h}(\boldsymbol{r}_0 - \boldsymbol{r}') \delta(\boldsymbol{r}_0 - \boldsymbol{r}' - \boldsymbol{r}) \\ &- \frac{1}{2} \iiint d\boldsymbol{r}_0 d\boldsymbol{r}' d\boldsymbol{r}'' \, \rho^*(\boldsymbol{r}_0) \rho^*(\boldsymbol{r}') \rho^*(\boldsymbol{r}'') \\ &\quad \times \Big[\Big\{ \widetilde{h}(\boldsymbol{r}_0 - \boldsymbol{r}') h(\boldsymbol{r}' - \boldsymbol{r}'') \delta(\boldsymbol{r}_0 - \boldsymbol{r}'' - \boldsymbol{r}) + \widetilde{h}(\boldsymbol{r}_0 - \boldsymbol{r}'') h(\boldsymbol{r}'' - \boldsymbol{r}') \delta(\boldsymbol{r}_0 - \boldsymbol{r}' - \boldsymbol{r}) \Big\} \\ &\qquad + \Big\{ c(\boldsymbol{r}_0 - \boldsymbol{r}'') \widetilde{h}(\boldsymbol{r}'' - \boldsymbol{r}') \delta(\boldsymbol{r}_0 - \boldsymbol{r}' - \boldsymbol{r}) + c(\boldsymbol{r}'' - \boldsymbol{r}_0) \widetilde{h}(\boldsymbol{r}_0 - \boldsymbol{r}') \delta(\boldsymbol{r}'' - \boldsymbol{r}' - \boldsymbol{r}) \Big\} \Big], \end{aligned} \tag{A63}$$

noting that $c(-\boldsymbol{r}) = c(\boldsymbol{r})$. The approximate relation (A61) can be readily used by rewriting Equation (A63) as

$$\frac{\delta \mathcal{L}(\widetilde{h})}{\delta \widetilde{h}(\boldsymbol{r})} = \frac{1}{2} \Big\{ \int d\boldsymbol{r}_0 \, \rho^*(\boldsymbol{r}_0) \rho^*(\boldsymbol{r}_0 - \boldsymbol{r}) E_{\mathrm{oz}}(\widetilde{h}) + \int d\boldsymbol{r}' \, \rho^*(\boldsymbol{r}' + \boldsymbol{r}) \rho^*(\boldsymbol{r}') E'_{\mathrm{oz}}(\widetilde{h}) \Big\}, \tag{A64}$$

where

$$\begin{aligned}&E_{\mathrm{oz}}(\widetilde{h}) \\ &= \widetilde{h}(\boldsymbol{r}) - \int d\boldsymbol{r}' \, \rho^*(\boldsymbol{r}') \widetilde{h}(\boldsymbol{r}_0 - \boldsymbol{r}') h(\boldsymbol{r}' - \boldsymbol{r}_0 + \boldsymbol{r}) - \int d\boldsymbol{r}'' \, \rho^*(\boldsymbol{r}'') c(\boldsymbol{r}_0 - \boldsymbol{r}'') \widetilde{h}(\boldsymbol{r}'' - \boldsymbol{r}_0 + \boldsymbol{r}) \end{aligned} \tag{A65}$$

and

$$\begin{aligned}&E'_{\mathrm{oz}}(\widetilde{h}) \\ &= \widetilde{h}(\boldsymbol{r}) - \int d\boldsymbol{r}'' \, \rho^*(\boldsymbol{r}'') \widetilde{h}(\boldsymbol{r}' + \boldsymbol{r} - \boldsymbol{r}'') h(\boldsymbol{r}'' - \boldsymbol{r}') - \int d\boldsymbol{r}_0 \, \rho^*(\boldsymbol{r}_0) c(\boldsymbol{r}' + \boldsymbol{r} - \boldsymbol{r}_0) \widetilde{h}(\boldsymbol{r}_0 - \boldsymbol{r}'). \end{aligned} \tag{A66}$$

It is found from Equation (A61) that $E_{\mathrm{oz}}(\widetilde{h}) = E'_{\mathrm{oz}}(\widetilde{h}) \approx \widetilde{c}(\boldsymbol{r})$, so that Equation (A64) becomes

$$\frac{\delta \mathcal{L}(\widetilde{h})}{\delta \widetilde{h}(\boldsymbol{r})} = \frac{1}{2} \Big\{ \int d\boldsymbol{r}_0 \, \rho^*(\boldsymbol{r}_0) \rho^*(\boldsymbol{r}_0 - \boldsymbol{r}) \widetilde{c}(\boldsymbol{r}) + \int d\boldsymbol{r}' \, \rho^*(\boldsymbol{r}' + \boldsymbol{r}) \rho^*(\boldsymbol{r}') \widetilde{c}(\boldsymbol{r}) \Big\}. \tag{A67}$$

Thus, we verify the first term on the rhs of Equation (36) by setting $\boldsymbol{r}_0 = \boldsymbol{r}' + \boldsymbol{r}$ in Equation (A67).

Appendix G. Derivation of Equation (44)

The result in Equation (44) is derived as follows:

$$\begin{aligned}
\mathcal{M}(\boldsymbol{k},\boldsymbol{q}) &= \frac{1}{S^2(\boldsymbol{q})\,S^2(\boldsymbol{k}-\boldsymbol{q})} - \frac{1}{S^2(\boldsymbol{q})} - \frac{1}{S^2(\boldsymbol{k}-\boldsymbol{q})} \\
&= \left\{\frac{1}{S^2(\boldsymbol{q})} - 1\right\}\left\{\frac{1}{S^2(\boldsymbol{k}-\boldsymbol{q})} - 1\right\} - 1 \\
&= \left\{\overline{\rho}^2 c_*^2(\boldsymbol{q}) - 2\overline{\rho}c_*(\boldsymbol{q})\right\}\left\{\overline{\rho}^2 c_*^2(\boldsymbol{k}-\boldsymbol{q}) - 2\overline{\rho}c_*(\boldsymbol{k}-\boldsymbol{q})\right\} - 1 \\
&= \left\{\overline{\rho}^2 c_*(\boldsymbol{q})c_*(\boldsymbol{k}-\boldsymbol{q})\right\}^2 + 2\overline{\rho}^2 c_*(\boldsymbol{q})c_*(\boldsymbol{k}-\boldsymbol{q})\{2 - \overline{\rho}c_*(\boldsymbol{q}) - \overline{\rho}c_*(\boldsymbol{k}-\boldsymbol{q})\} - 1 \\
&= \left\{\overline{\rho}^2 c_*(\boldsymbol{q})c_*(\boldsymbol{k}-\boldsymbol{q})\right\}^2 + 2\overline{\rho}^2 c_*(\boldsymbol{q})c_*(\boldsymbol{k}-\boldsymbol{q})\left\{\frac{1}{S(\boldsymbol{q})} + \frac{1}{S(\boldsymbol{k}-\boldsymbol{q})}\right\} - 1, \qquad \text{(A68)}
\end{aligned}$$

where use has been made of the relation, $S(\boldsymbol{q}) = \{1 - \overline{\rho}c_*(\boldsymbol{q})\}^{-1}$, in the last line.

References

1. Cavagna, A. Supercooled liquids for pedestrians. *Phys. Rep.* **2009**, *476*, 51–124. [CrossRef]
2. Berthier, L.; Biroli, G. Theoretical perspective on the glass transition and amorphous materials. *Rev. Mod. Phys.* **2011**, *83*, 587–645. [CrossRef]
3. Hunter, G.L.; Weeks, E.R. The physics of the colloidal glass transition. *Rep. Prog. Phys.* **2012**, *75*, 066501. [CrossRef] [PubMed]
4. Biroli, G.; Garrahan, J.P. Perspective: The glass transition. *J. Chem. Phys.* **2013**, *138*, 12A301. [CrossRef]
5. Arceri, F.; Landes, F.P.; Berthier, L.; Biroli, G. Glasses and aging: A statistical mechanics perspective. In *Statistical and Nonlinear Physics*; Chakraborty, B., Ed.; Springer: New York, NY, USA, 2022; pp. 229–296.
6. Berthier, L.; Reichman, D.R. Modern computational studies of the glass transition. *Nat. Rev. Phys.* **2023**, *5*, 102–116. [CrossRef]
7. Berthier, L.; Biroli, G.; Bouchaud, J.P.; Kob, W.; Miyazaki, K.; Reichman, D.R. Spontaneous and induced dynamic fluctuations in glass formers. I. General results and dependence on ensemble and dynamics. *J. Chem. Phys.* **2007**, *126*, 184503. [CrossRef] [PubMed]
8. Berthier, L.; Biroli, G.; Bouchaud, J.P.; Kob, W.; Miyazaki, K.; Reichman, D.R. Spontaneous and induced dynamic correlations in glass formers. II. Model calculations and comparison to numerical simulations. *J. Chem. Phys.* **2007**, *126*, 184504. [CrossRef] [PubMed]
9. Laudicina, C.C.; Luo, C.; Miyazaki, K.; Janssen, L.M. Dynamical susceptibilities near ideal glass transitions. *Phys. Rev. E* **2022**, *106*, 064136. [CrossRef]
10. Biroli, G.; Charbonneau, P.; Folena, G.; Hu, Y.; Zamponi, F. Local dynamical heterogeneity in simple glass formers. *Phys. Rev. Lett.* **2022**, *128*, 175501. [CrossRef] [PubMed]
11. Biroli, G.; Miyazaki, K.; Reichman, D.R. Dynamical heterogeneity in glass-forming liquids. In *Spin Glass Theory and Far Beyond: Replica Symmetry Breaking after 40 Years*; Marinari, E., Mézard, M., Parisi, G., Ricci-Tersenghi, F., Sicuro, G., Zamponi, F., Eds.; World Scientific: Singapore, 2023; pp. 187–201.
12. Bhattacharyya, S.M.; Bagchi, B.; Wolynes, P.G. Facilitation, complexity growth, mode coupling, and activated dynamics in supercooled liquids. *Proc. Natl. Acad. Sci. USA* **2008**, *105*, 16077–16082. [CrossRef]
13. Chandler, D.; Garrahan, J.P. Dynamics on the way to forming glass: Bubbles in space-time. *Annu. Rev. Phys. Chem.* **2010**, *61*, 191–217. [CrossRef] [PubMed]
14. Ozawa, M.; Biroli, G. Elasticity, Facilitation, and Dynamic Heterogeneity in Glass-Forming Liquids. *Phys. Rev. Lett.* **2023**, *130*, 138201. [CrossRef] [PubMed]
15. Das, S.P. Mode-coupling theory and the glass transition in supercooled liquids. *Rev. Mod. Phys.* **2004**, *76*, 785–851. [CrossRef]
16. Janssen, L.M. Mode-coupling theory of the glass transition: A primer. *Front. Phys.* **2018**, *6*, 97. [CrossRef]
17. Lubchenko, V.; Wolynes, P.G. Theory of structural glasses and supercooled liquids. *Annu. Rev. Phys. Chem.* **2007**, *58*, 235–266. [CrossRef] [PubMed]
18. Parisi, G.; Zamponi, F. Mean-field theory of hard sphere glasses and jamming. *Rev. Mod. Phys.* **2010**, *82*, 789–845. [CrossRef]
19. Kirkpatrick, T.R.; Thirumalai, D. Colloquium: Random first order transition theory concepts in biology and Physics. *Rev. Mod. Phys.* **2015**, *87*, 183–209. [CrossRef]
20. Biroli, G.; Bouchaud, J.P. The RFOT Theory of Glasses: Recent Progress and Open Issues. *C. R. Phys.* **2023**, *24*, 1–15. [CrossRef]
21. Bouchaud, J.P.; Biroli, G. On the Adam-Gibbs-Kirkpatrick-Thirumalai-Wolynes scenario for the viscosity increase in glasses. *J. Chem. Phys.* **2004**, *121*, 7347–7354. [CrossRef]
22. Berthier, L.; Tarjus, G. Testing "microscopic" theories of glass-forming liquids. *Eur. Phys. J. E Soft Matter* **2011**, *34*, 1–10. [CrossRef]
23. Banerjee, A.; Sengupta, S.; Sastry, S.; Bhattacharyya, S.M. Role of structure and entropy in determining differences in dynamics for glass formers with different interaction potentials. *Phys. Rev. Lett.* **2014**, *113*, 225701. [CrossRef]

24. Banerjee, A.; Nandi, M.K.; Sastry, S.; Bhattacharyya, S.M. Effect of total and pair configurational entropy in determining dynamics of supercooled liquids over a range of densities. *J. Chem. Phys.* **2016**, *145*, 034502. [CrossRef]
25. Landes, F.P.; Biroli, G.; Dauchot, O.; Liu, A.J.; Reichman, D.R. Attractive versus truncated repulsive supercooled liquids: The dynamics is encoded in the pair correlation function. *Phys. Rev. E* **2020**, *101*, 010602. [CrossRef]
26. Nandi, M.K.; Bhattacharyya, S.M. Microscopic theory of softness in supercooled liquids. *Phys. Rev. Lett.* **2021**, *126*, 208001. [CrossRef] [PubMed]
27. Singh, A.; Singh, Y. How attractive and repulsive interactions affect structure ordering and dynamics of glass-forming liquids. *Phys. Rev. E* **2021**, *103*, 052105. [CrossRef] [PubMed]
28. Sharma, M.; Nandi, M.K.; Bhattacharyya, S.M. A comparative study of the correlation between the structure and the dynamics for systems interacting via attractive and repulsive potentials. *J. Chem. Phys.* **2023**, *159*, 104502. [CrossRef]
29. Kirkpatrick, T.R.; Wolynes, P.G. Connections between some kinetic and equilibrium theories of the glass transition. *Phys. Rev. A* **1987**, *35*, 3072–3080. [CrossRef] [PubMed]
30. Monasson, R. Structural glass transition and the entropy of the metastable states. *Phys. Rev. Lett.* **1995**, *75*, 2847–2850. [CrossRef] [PubMed]
31. Mézard, M.; Parisi, G. Thermodynamics of glasses: A first principles computation. *J. Phys. Condens. Matter* **1999**, *11*, A157. [CrossRef]
32. Mangeat, M.; Zamponi, F. Quantitative approximation schemes for glasses. *Phys. Rev. E* **2016**, *93*, 012609. [CrossRef] [PubMed]
33. Mézard, M.; Parisi, G. A tentative replica study of the glass transition. *J. Phys. A Math. Gen.* **1996**, *29*, 6515–6524. [CrossRef]
34. Ikeda, A.; Miyazaki, K. Mode-coupling theory as a mean-field description of the glass transition. *Phys. Rev. Lett.* **2010**, *104*, 255704. [CrossRef]
35. Franz, S.; Jacquin, H.; Parisi, G.; Urbani, P.; Zamponi, F. Quantitative field theory of the glass transition. *Proc. Natl. Acad. Sci. USA* **2012**, *109*, 18725–18730. [CrossRef]
36. Franz, S.; Jacquin, H.; Parisi, G.; Urbani, P.; Zamponi, F. Static replica approach to critical correlations in glassy systems. *J. Chem. Phys.* **2013**, *138*, 12A540. [CrossRef] [PubMed]
37. Jaquin, H.; Zamponi, F. Systematic expansion in the order parameter for replica theory of the dynamical glass transition. *J. Chem. Phys.* **2013**, *138*, 12A542. [CrossRef] [PubMed]
38. Biroli, G.; Cammarota, C.; Tarjus, G.; Tarzia, M. Random field Ising-like effective theory of the glass transition. II. Finite-dimensional models. *Phys. Rev. B* **2018**, *98*, 174206. [CrossRef]
39. Singh, Y.; Stoessel, J.P.; Wolynes, P.G. Hard-sphere glass and the density-functional theory of aperiodic crystals. *Phys. Rev. Lett.* **1985**, *54*, 1059–1062. [CrossRef] [PubMed]
40. Dasgupta, C. Glass transition in the density functional theory of freezing. *Europhys. Lett.* **1992**, *20*, 131–136. [CrossRef]
41. Xia, X.; Wolynes, P.G. Fragilities of liquids predicted from the random first order transition theory of glasses. *Proc. Natl. Acad. Sci. USA* **2000**, *97*, 2990–2994. [CrossRef]
42. Kaur, C.; Das, S.P. Heterogeneities in supercooled liquids: A density-functional study. *Phys. Rev. Lett.* **2001**, *86*, 2062–2065. [CrossRef]
43. Kaur, C.; Das, S.P. Metastable structures with modified weighted density-functional theory. *Phys. Rev. E* **2002**, *65*, 026123. [CrossRef]
44. Kim, K.; Munakata, T. Glass transition of hard sphere systems: Molecular dynamics and density functional theory. *Phys. Rev. E* **2003**, *68*, 021502. [CrossRef]
45. Chaudhuri, P.; Karmakar, S.; Dasgupta, C.; Krishnamurthy, H.R.; Sood, A.K. Equilibrium glassy phase in a polydisperse hard-sphere system. *Phys. Rev. Lett.* **2005**, *95*, 248301. [CrossRef] [PubMed]
46. Chaudhuri, P.; Karmakar, S.; Dasgupta, C. Signatures of dynamical heterogeneity in the structure of glassy free-energy minima. *Phys. Rev. Lett.* **2008**, *100*, 125701. [CrossRef] [PubMed]
47. Singh, S.L.; Bharadwaj, A.S.; Singh, Y. Free-energy functional for freezing transitions: Hard-sphere systems freezing into crystalline and amorphous structures. *Phys. Rev. E* **2011**, *83*, 051506. [CrossRef] [PubMed]
48. Lubchenko, V. Theory of the structural glass transition: A pedagogical review. *Adv. Phys.* **2015**, *64*, 283–443. [CrossRef]
49. Odagaki, T. Non-equilibrium statistical mechanics based on the free energy landscape and its application to glassy systems. *J. Phys. Soc. Jpn.* **2017**, *86*, 082001. [CrossRef]
50. Mondal, A.; Premkumar, L.; Das, S.P. Dependence of the configurational entropy on amorphous structures of a hard-sphere fluid. *Phys. Rev. E* **2017**, *96*, 012124. [CrossRef] [PubMed]
51. Mondal, A.; Das, S.P. A classical density functional theory model for fragility in the hard-sphere limit. *Prog. Theor. Phys.* **2020**, *2020*, 073I02. [CrossRef]
52. Leishangthem, P.; Ahmad, F.; Das, S.P. Localization, disorder, and entropy in a coarse-grained Model of the amorphous solid. *Entropy* **2021**, *23*, 1171. [CrossRef]
53. Kirkpatrick, T.R.; Thirumalai, D. Random solutions from a regular density functional hamiltonian: A static and dynamical theory for the structural glass transition. *J. Phys. A Math. Gen.* **1989**, *22*, L149. [CrossRef]
54. Lafuente, L.; Cuesta, J.A. First-principles derivation of density-functional formalism for quenched-annealed systems. *Phys. Rev. E* **2006**, *74*, 041502. [CrossRef] [PubMed]

55. Dzero, M.; Schmalian, J.; Wolynes, P.G. Replica theory for fluctuations of the activation barriers in glassy systems. *Phys. Rev. B* **2009**, *80*, 024204. [CrossRef]
56. Vardhan, P.; Das, S.P. Configurational entropy from a replica approach: A density-functional model. *Phys. Rev. E* **2022**, *105*, 024110. [CrossRef]
57. Vardhan, P.; Das, S.P. Complexity calculation for an amorphous metastable solid. *J. Non-Cryst.* **2022**, *597*, 121744. [CrossRef]
58. Evans, R. The nature of the liquid-vapour interface and other topics in the statistical mechanics of non-uniform, classical fluids. *Adv. Phys.* **1979**, *28*, 143–200. [CrossRef]
59. Singh, Y. Density-functional theory of freezing and properties of the ordered phase. *Phys. Rep.* **1991**, *207*, 351–444. [CrossRef]
60. Löwen, H. Melting, freezing and colloidal suspensions. *Phys. Rep.* **1994**, *237*, 249–324. [CrossRef]
61. Ramakrishnan, T.V.; Yussouff, M. First-principles order-parameter theory of freezing. *Phys. Rev. B* **1979**, *19*, 2775. [CrossRef]
62. Hansen, J.-P.; McDonald, I.R. *Theory of Simple Liquids*, 3rd ed.; Elsevier: Amsterdam, The Netherlands, 2006.
63. Bomont, J.M. Recent advances in the field of integral equation theories: Bridge functions and applications to classical fluids. *Adv. Chem. Phys.* **2008**, *139*, 1–84.
64. Morita, T.; Hiroike, K. A new approach to the theory of classical fluids. III: General treatment of classical systems. *Prog. Theor. Phys.* **1961**, *25*, 537–578. [CrossRef]
65. Franz, S.; Parisi, G. Phase diagram of coupled glassy systems: A mean-field study. *Phys. Rev. Lett.* **1997**, *79*, 2486–2489. [CrossRef]
66. Franz, S.; Parisi, G. Effective potential in glassy systems: Theory and simulations. *Phys. A Stat. Mech.* **1998**, *261*, 317–339. [CrossRef]
67. Cardenas, M.; Franz, S.; Parisi, G. Constrained Boltzmann-Gibbs measures and effective potential for glasses in hypernetted chain approximation and numerical simulations. *J. Chem. Phys.* **1999**, *110*, 1726–1734. [CrossRef]
68. Berthier, L. Overlap fluctuations in glass-forming liquids. *Phys. Rev. E* **2013**, *88*, 022313. [CrossRef] [PubMed]
69. Charbonneau, P.; Kurchan, J.; Parisi, G.; Urbani, P.; Zamponi, F. Glass and jamming transitions: From exact results to finite-dimensional descriptions. *Annu. Rev. Condens. Matter Phys.* **2017**, *8*, 265–288. [CrossRef]
70. Bomont, J.M.; Pastore, G.; Hansen, J.P. Coexistence of low and high overlap phases in a supercooled liquid: An integral equation investigation. *J.Chem. Phys.* **2019**, *146*, 114504. [CrossRef]
71. Guiselin, B.; Tarjus, G.; Berthier, L. On the overlap between configurations in glassy liquids. *J. Chem. Phys.* **2020**, *153*, 224502. [CrossRef]
72. Berthier, L. Self-induced heterogeneity in deeply supercooled liquids. *Phys. Rev. Lett.* **2021**, *127*, 088002. [CrossRef]
73. Guiselin, B.; Berthier, L.; Tarjus, G. Statistical mechanics of coupled supercooled liquids in finite dimensions. *SciPost Phys.* **2022**, *12*, 091. [CrossRef]
74. Guiselin, B.; Tarjus, G.; Berthier, L. Static self-induced heterogeneity in glass-forming liquids: Overlap as a microscope. *J. Chem. Phys.* **2022**, *156*, 194503. [CrossRef]
75. Folena, G.; Biroli, G.; Charbonneau, P.; Hu, Y.; Zamponi, F. Equilibrium fluctuations in mean-field disordered models. *Phys. Rev. E* **2022**, *106*, 024605. [CrossRef]
76. Zhou, S.; Ruckenstein, E. High-order direct correlation functions of uniform fluids and their application to the high-order perturbative density functional theory. *Phys. Rev. E* **2000**, *61*, 2704. [CrossRef]
77. Choudhury, N.; Patra, C.N.; Ghosh, S.K. A new perturbative weighted density functional theory for an inhomogeneous hard–sphere fluid mixture. *J. Phys. Condens.* **2002**, *14*, 11955. [CrossRef]
78. Zhou, S.; Jamnik, A. Further test of third order + second-order perturbation DFT approach: Hard core repulsive yukawa fluid subjected to diverse external fields. *J. Phys. Chem. B* **2006**, *110*, 6924–6932. [CrossRef] [PubMed]
79. Negele, J.W.; Orland, H. *Quantum Many-Particle Systems*; Pines, D., Ed.; Taylor & Francis: Reading, MA, USA, 1998.
80. Fredrickson, G.H.; Ganesan, V.; Drolet, F. Field-theoretic computer simulation methods for polymers and complex fluids. *Macromolecules* **2002**, *35*, 16–39. [CrossRef]
81. Delaney, K.T.; Fredrickson, G.H. Recent developments in fully fluctuating field-theoretic simulations of polymer melts and solutions. *J. Phys. Chem. B* **2016**, *120*, 7615–7634. [CrossRef] [PubMed]
82. Matsen, M.W. Self-consistent field theory and its applications. In *Soft Matter 1*; Gompper, G., Schick, M., Eds.; Wiley-VCH: Weinheim, Germany, 2006; Volume 1, pp. 87–178.
83. Parisi, G. Euclidean random matrices: Solved and open problems. In *Application of Random Matrices in Physics, NATO Science Series II: Mathematics, Physics and Chemistry 221*; Brézin, É., Kazakov, V., Serban, D., Wiegmann, P., Zabrodin, A., Eds.; Springer: New York, NY, USA, 2006; pp. 219–260.
84. Frusawa, H.; Hayakawa, R. Field theoretical representation of the Hohenberg-Kohn free energy for fluids. *Phys. Rev. E* **1999**, *60*, R5048. [CrossRef] [PubMed]
85. Frusawa, H. Free-energy functional of instantaneous correlation field in liquids: Field-theoretic derivation of the closures. *Phys. Rev. E* **2020**, *102*, 012117. [CrossRef]
86. Frusawa, H. Self-consistent field theory of density correlations in classical fluids. *Phys. Rev. E* **2018**, *98*, 052130. [CrossRef]
87. Woo, H.J.; Song, X. Functional integral formulations for classical fluids. *J. Chem. Phys.* **2001**, *114*, 5637–5641. [CrossRef]
88. Patsahan, O.; Mryglod, I. The method of collective variables: A link with the density functional theory. *Condens. Matter Phys.* **2012**, *15*, 24001. [CrossRef]

89. Frusawa, H.; Hayakawa, R. On the controversy over the stochastic density functional equations. *J. Phys. A Math. Gen.* **2000**, *33*, L155. [CrossRef]
90. Archer, A.J.; Rauscher, M. Dynamical density functional theory for interacting Brownian particles: Stochastic or deterministic? *J. Phys. A Math. Gen.* **2004**, *37*, 9325. [CrossRef]
91. te Vrugt, M.; Löwen, H.; Wittkowski, R. Classical dynamical density functional theory: From fundamentals to applications. *Adv. Phys.* **2020**, *69*, 121–247. [CrossRef]
92. Frusawa, H. Bridging the gap between correlation entropy functionals in the mean spherical and the hypernetted chain approximations: A field theoretic description. *J. Phys. A Math. Theor.* **2018**, *52*, 015003. [CrossRef]
93. Bäumchen, O.; McGraw, J.D.; Forrest, J.A.; Dalnoki-Veress, K. Reduced glass transition temperatures in thin polymer films: Surface effect or artifact? *Phys. Rev. Lett.* **2012**, *109*, 055701. [CrossRef] [PubMed]
94. Napolitano, S.; Glynos, E.; Tito, N.B. Glass transition of polymers in bulk, confined geometries, and near interfaces. *Rep. Prog. Phys.* **2017**, *80*, 036602. [CrossRef] [PubMed]
95. Frusawa, H. Non-hyperuniform metastable states around a disordered hyperuniform state of densely packed spheres: Stochastic density functional theory at strong coupling. *Soft Matter* **2021**, *17*, 8810–8831. [CrossRef] [PubMed]

Disclaimer/Publisher's Note: The statements, opinions and data contained in all publications are solely those of the individual author(s) and contributor(s) and not of MDPI and/or the editor(s). MDPI and/or the editor(s) disclaim responsibility for any injury to people or property resulting from any ideas, methods, instructions or products referred to in the content.